Institute of Space and Aeronautical Science, University of Tokyo
Report No. 589, January 1981

Acoustic Radiation of Inlet-Turbulence/Rotor Interaction in Free and Ducted Spaces

By

Susumu KOTAKE

Summary: The far-field acoustic radiation caused by the inlet-turbulence/fan-rotor interaction in free and ducted spaces is studied theoretically. Incompressible, two-dimensional unsteady thin-airfoil theory is combined with an acoustic radiation model of concentrated point dipoles. The effect of duct termination is neglected. The far-field power spectral density of the associated sound is largely affected by the nature of the incoming turbulence. The effects of the turbulence scale, rotor speed, duct length and the mean flow upon the frequency spectrum and directivity are investigated in both cases of free-space and ducted-space in which "cut-off" and "cut-on" modes have coupled contributions to the radiation field.

CONTENTS

NOMENCLATURE

A_m	mode amplitude coefficient
a	speed of sound
$\boldsymbol{a}_\nu$	position vector of ν-th dipole
B	blade number

b	blade span
c	blade chord
$E\{\ \}$	ensemble average
$\boldsymbol{F}$	Fourier transform ot
$\boldsymbol{f}$	force per unit volume $\boldsymbol{f}$
G	Fourier transform of g
g	Green's function
J	Bessel function of first kind
k	acoustic wave number, ω/a, (kR)
k_{mn}	mode cross-section wave number
$\boldsymbol{L}$	concentrated lift force
$\mathscr{L}_x$	axial turbulence scale $(\mathscr{L}_x/R)$
l	duct length (l/R)
M	flow Mach number, U/a
m, n	circumferential and radial mode numbers
P	Fourier transform of p
p	acoustic pressure
R	duct radius
R_e	effective radial position of point dipole (R_e/R)
S_p	power spectral density of acoustic pressure
$\bar{S}_p$	nondimensionalized S_p, Eq. (57)
S_e	power spectral density of Sears function
S_l	power spectral density of fluctuating lift
s_{mn}	defined in Table 1
t	time
U	velocity of mean flow
V	flow velocity relative to rotor, Eq. (45)
u, v	turbulent velocity
$\boldsymbol{x}$	position vector of observer $(\|\boldsymbol{x}\|, \Theta, \Phi)$
x, y, z	Catesian coordinates (x along rotor axis)
x, r, θ	cylindrical coordinates
α	blade angle
β	$=\sqrt{1-M^2}$
β_w	specific acoustic admittance of duct wall
Λ_{mn}	defined by Eq. (14)
$\delta(\ )$	Dirac delta function
κ_{mn}	mode axial wave number, defined in Table 1
ρ	density
Φ	azimuth angle between observer and rotor-axis
Ω	angular velocity of rotor $(\Omega R/a)$
ω	circular frequency $(\omega R/a)$
$\bar{\omega}$	reduced frequency, $\omega c/V$

Superscripts

*	complex conjugate
(D)	ducted-space case
(F)	free-space case

Subscripts

o	acoustic source
x	axial component
θ	circumferential component
ν	ν-th blade

NOTE:
Dimensionless quantities are denoted in ( ).

1. INTRODUCTION

Since the problem caused by compressor and fan has become severe with the introduction of high bypass ratio fan-jet engines, theoretical studies for the noise prediction and control have already accomplished with promissing results. The associated noise is however the product of a long chain of cause and effect, which is under the influence of a large number of parameters such as geometric configuration of blade and duct, aerodynamic characteristics of blade, flow fields in and out of the duct, acoustic characteristics of duct walls, and so on. It is extremely difficult to predict the contribution of each parameter to the acoustic radiation field in consideration of all these parameters.

Fluctuating lift forces on the blades caused by stationary distortion or turbulence of incoming flows have a considerable effect upon the associated sound generation because they can radiate appreciable acoustic energy compared with steady forces except for fans with a high tip speed. The mechanisms by which inlet turbulence might produce noise are well-understood. The non-uniformity in space and time of velocity associated with the convected turbulence produces non-stationary fluctuations of forces on a blade leading to acoustic radiation.

The effects of the unsteady force or mass distrubtions on blades caused by stationary distortion of incoming flows have considerably studied in both cases of free-field and ducted fans, since they have high radiation efficiency to produce strong tones at shaft rotational frequency due to the characteristics of their large spatial coherence. In practice, however, even with elaborate inlet ducting, there are additional and inevitable turbulent velocity fluctuations which may be still important sound-generating sources.

Mani [*1*] studied analytically the problem of sound generation due to free stream turbulence incident on a two-dimensional rotor or stator row, assuming turbulence to be homogeneous, isotropic and stationary. Chandrashekhara [*2*] made a theoretical and experimental study of estimating the sound radiated by fluctuating forces on blades of a fan in free-space due to inlet turbulence which was characterized by detailed flow measurements. Hanson [*3*] studied the acoustic radiation of fans in free-space due to inflow turbulence which was not necessarily homogeneous and isotropic, using random pulse modulation theory. Amiet [*4*] showed a theoretical expression for

the far-field acoustic power spectral density produced by an airfoil in a subsonic turbulent flow with a good agreement with experimental measurements available in the liturature.

The problem of noise generated by a fan operating in some kind of duct is of most commly encountered types. The presence of duct system, reflecting and/or absorbing surfaces, affects and modifies considerably the near and far fields of associated sound radiation. In this cases, the radiation from each blade combines to make acoustic modes in the duct, propagates through the duct with the efficiency of each mode, and radiates from the duct ends into the free-field. At the duct end, some degrees of coupling modes with reflection back up the duct must be taken into account, although modes excited well above their cut-off frequency tend to be less coupled with other modes. On this respect, detailed studies of the sound field both inside and outside a duct of semi-infinite or finite length have been done by many investigators [*5*, *6*]. Although the coupling of modes at the duct ends is substantial for the real problems of sound radiation caused by fans and compressors, the assumption of no mode-coupling at the duct ends leads to a very appreciable gain in computational simplicity with fruitfull results. It can split a lengthy calculation dependent upon the conditions both inside and outside the duct into two independent serial calculations and help on understanding of a basic aspect of sound radiation problem.

The prediction of the acoustic modes in duct caused by inlet-turbulence and rotor interaction further requires the statistical knowledge of inlet-turbulence and the unsteady lift response of blade to the incident velocity field. The turbulence properties of incoming flows usually encountered are closely approximated by an isotropic homogeneous turbulence model. The most widely used models of isotropic turbulence are the Kármán and the Liepmann models. On the other hand, the most usefull theoretical method of estimating aerodynamic lift in unsteady incompressible flow is the Kármán-Sears theory for the lift of an infinite single airfoil due to convected sinusoidal gusts, which can be applied directly to blade operating in two-dimensional incompressible incident turbulent flows. To use this simple relation for the case of blade rotating in a duct, many factors remain to be unknown such as spanwise variation in the upwash field, the three-dimensional effect of the finite span of blade, the effect of compressibility, etc. Although there are extended theories to include these effects, as far as sound radiation is concerned, this incompressible two-dimensional thin airfoil theory has the advantage of a very simple closed form expression of lift response and may be most effective in the range of acoustic wave length larger than the blade chord and smaller than the blade span.

In the present study, the incompressible two-dimensional unsteady air-foil theory is combined with an acoustic radiation model in which each blade is regarded as an equivalent point force, and the propagating modes in the duct are linked to the far field radiation from an open end of the duct without any coupling between modes. The far fields of acoustic radiation caused by the inlet-turbulence and fan-rotor interaction are investigated theoretically.

2. Far-Field Acoustic Radiation by Random Rotor-Blade Loading in Circular Duct

2.1 *Sound Pressure in an Infinite Cylindrical Duct*

Let x denote the coordinate along the duct axis, and r, θ denote cross-section position coordinates as shown in Fig. 1. The wave equation for the acoustic pressure p

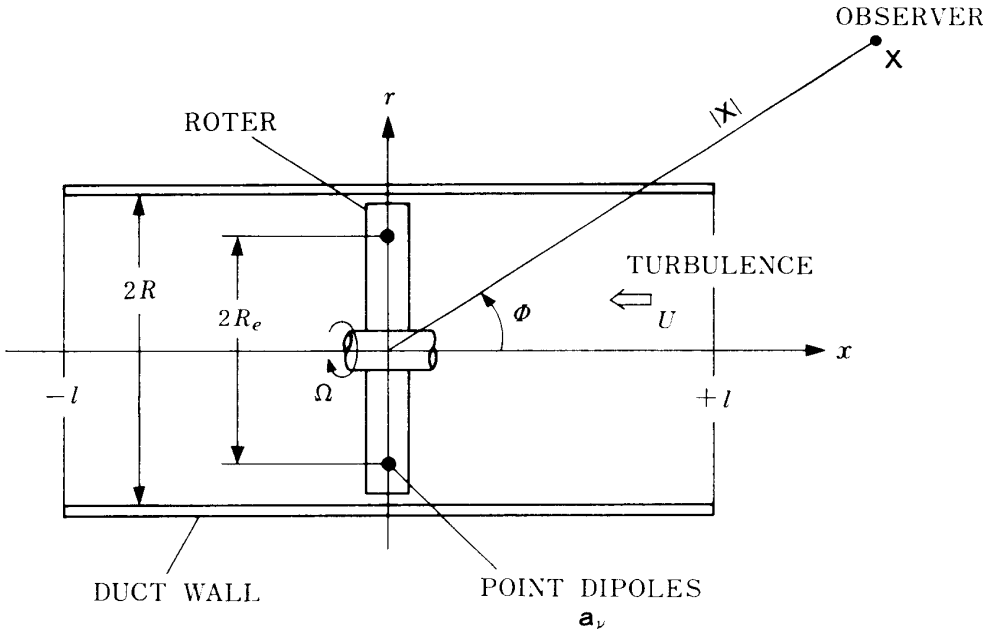

(a) Ducted space

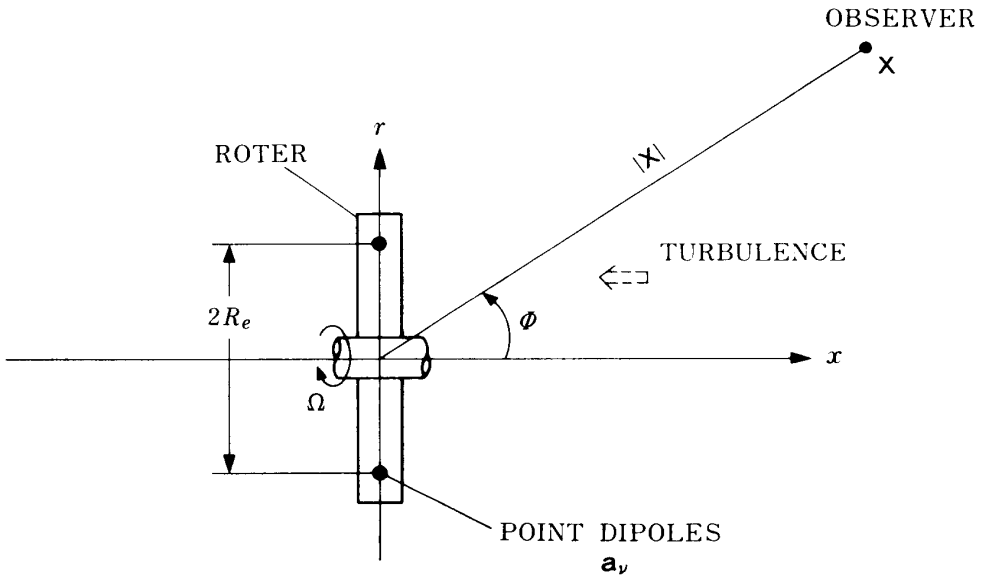

(b) Free space

Fig. 1. Coordinate system of a rotor in ducted and free spaces.

in a uniform acoustic medium with uniform mean flow U and acted by a distribution of dipole force $\boldsymbol{f}$ is given by

$$\nabla^2 p(\boldsymbol{r}, t)-\frac{1}{a^2}\left(\frac{\partial}{\partial t}-U\frac{\partial}{\partial x}\right)^2 p(\boldsymbol{r}, t)=\nabla\cdot\boldsymbol{f}(\boldsymbol{r}, t) \tag{1}$$

where ∇ and ∇^2 in the cylindrical coordinates $\boldsymbol{r}(x, r, \theta)$ are respectively

$$\nabla=\left(\frac{\partial}{\partial x}, \frac{\partial}{\partial r}, \frac{1}{r}\frac{\partial}{\partial \theta}\right)$$

$$\nabla^2=\frac{\partial^2}{\partial x^2}+\frac{\partial^2}{\partial r^2}+\frac{1}{r}\frac{\partial}{\partial r}+\frac{1}{r^2}\frac{\partial^2}{\partial \theta^2}.$$

The acoustic particle velocity is related to the acoustic pressure by the equation of motion

$$\rho\left(\frac{\partial}{\partial t}-U\frac{\partial}{\partial x}\right)\boldsymbol{v}=-\nabla p, \tag{2}$$

where ρ is the mean density of the medium. For a duct wall having the radius R and the specific acoustic admittance $\beta_w(=\rho a v_r/p)$ at $r=R$, the boundary condition of Eq. (1) is thus given by

$$\left[\frac{\beta_w}{a}\left(\frac{\partial}{\partial t}-U\frac{\partial}{\partial x}\right)p(\boldsymbol{r}, t)\right]_{r=R}=-\left[\frac{\partial p(\boldsymbol{r}, t)}{\partial r}\right]_{r=R}. \tag{3}$$

By assuming the existence of following Fourier transforms of $p(\boldsymbol{r}, t)$ and $\boldsymbol{f}(\boldsymbol{r}, t)$ (See NOTE)

$$P(\boldsymbol{r}, \omega)=\frac{1}{2\pi}\int_{-\infty}^{\infty} p(\boldsymbol{r}, t)e^{-i\omega t}dt \tag{4}$$

$$\boldsymbol{F}(\boldsymbol{r}, \omega)=\frac{1}{2\pi}\int_{-\infty}^{\infty} \boldsymbol{f}(\boldsymbol{r}, t)e^{-i\omega t}dt \tag{5}$$

Eqs. (1) and (3) can be rewritten in the Fourier time-transform as

$$\nabla^2 P(\boldsymbol{r}, \omega)-\left(ik-M\frac{\partial}{\partial x}\right)^2 P(\boldsymbol{r}, \omega)=\nabla\cdot\boldsymbol{F}(\boldsymbol{r}, \omega) \tag{6}$$

$$\left[\beta_w\left(ik-M\frac{\partial}{\partial x}\right)P(\boldsymbol{r}, \omega)\right]_{r=R}=-\left[\frac{\partial P(\boldsymbol{r}, \omega)}{\partial r}\right]_{r=R} \tag{7}$$

NOTE: For mathematical strictness, a stochastic Fourier-Stieltjes integral of type

$$p(\boldsymbol{r}, t)=\int dP(\boldsymbol{r}, \omega)e^{i\omega t}$$

should be used. As far as concerned with statistical quantities such as correlation or expected values, however, both methods yield the same result provided the statistical orthogonality condition can be assumed

$$\overline{dP(\omega)\cdot dP^*(\omega')}=\delta(\omega'-\omega)\overline{PP(\omega)}d\omega d\omega'.$$

where

$$k=\frac{\omega}{a}, \qquad M=\frac{U}{a}.$$

To solve Eqs. (1) and (3), or (6) and (7), it is convenient to introduce the concept of Green's function $g(\boldsymbol{r}, t; \boldsymbol{r}_0, t_0)$ which is defined as a solution of the same wave equation as Eq. (1) having an acoustic source of Dirac delta unit strength at $(\boldsymbol{r}_0, t_0)$

$$\nabla^2 g(\boldsymbol{r}, t; \boldsymbol{r}_0, t_0)-\frac{1}{a^2}\left(\frac{\partial}{\partial t}-U\frac{\partial}{\partial x}\right)^2 g(\boldsymbol{r}, t; \boldsymbol{r}_0, t_0)$$
$$=-\delta(\boldsymbol{r}-\boldsymbol{r}_0)\delta(t-t_0) \tag{8}$$

where

$$\delta(\boldsymbol{r}-\boldsymbol{r}_0)=\frac{1}{r}\delta(x-x_0)\delta(r-r_0)\delta(\theta-\theta_0),$$

and satisfies the same boundary condition as Eq. (3)

$$\left[\frac{\beta_w}{a}\left(\frac{\partial}{\partial t}-U\frac{\partial}{\partial x}\right)g(\boldsymbol{r}, t; \boldsymbol{r}_0, t_0)\right]_{r=R}=-\left[\frac{\partial}{\partial r}g(\boldsymbol{r}, t; \boldsymbol{r}_0, t_0)\right]_{r=R}. \tag{9}$$

Since the time dependence of the Green's function is in the form of $(t-t_0)$

$$g(\boldsymbol{r}, t; \boldsymbol{r}_0, t_0)=g(\boldsymbol{r}; \boldsymbol{r}_0, t-t_0),$$

the following Fourier time-transform of the Green's function corresponding to Eq. (4) can be defined.

$$G(\boldsymbol{r}; \boldsymbol{r}_0, \omega)=\frac{1}{2\pi}\int_{-\infty}^{\infty} g(\boldsymbol{r}; \boldsymbol{r}_0, \tau)e^{-i\omega\tau}d\tau. \tag{10}$$

The Fourier time-transforms of Eqs. (8) and (9) are then, respectively,

$$\nabla^2 G(\boldsymbol{r}; \boldsymbol{r}_0, \omega)-\left(ik-M\frac{\partial}{\partial x}\right)G(\boldsymbol{r}; \boldsymbol{r}_0, \omega)=-\delta(\boldsymbol{r}-\boldsymbol{r}_0) \tag{11}$$

$$\left[\beta_w\left(ik-M\frac{\partial}{\partial x}\right)G(\boldsymbol{r}; \boldsymbol{r}_0, \omega)\right]_{r=R}=-\left[\frac{\partial}{\partial r}G(\boldsymbol{r}; \boldsymbol{r}_0\, \omega)\right]_{r=R} \tag{12}$$

of which the solution can be given by a series of Bessel functions as follows (Appendix A)

$$G(\boldsymbol{r}; \boldsymbol{r}_0, \omega)=\frac{1}{i2\pi R^2}\sum_{m=-\infty}^{\infty}\sum_{n=0}^{\infty}\frac{1}{\Lambda_{mn}s_{mn}}J_m(k_{mn}r_0)J_m(k_{mn}r)$$
$$\cdot\exp\{-im(\theta-\theta_0)-i\kappa_{mn}(x-x_0)\} \tag{13}$$

where J_m is the Bessel function of the first kind of m-th order, s_{mn} and κ_{mn} are functions of M, k and k_{mn}, defined in Table 1,

TABLE 1. κ_{mn} and $s_{m\mu}$

κ_{mn}	$x-x_0>0$	$x-x_0<0$
$\lvert k\rvert<k_{mn}$	$\frac{k}{\beta^2}\left\{M+\sqrt{1-\beta^2\left(\frac{k_{mn}}{k}\right)^2}\right\}$	$\frac{k}{\beta^2}\left\{M-\sqrt{1-\beta^2\left(\frac{k_{mn}}{k}\right)^2}\right\}$
$k_{mn}\geqslant\lvert k\rvert\geqslant\beta k_{mn}$	$\frac{k}{\beta^2}\left\{M\pm\sqrt{1-\beta^2\left(\frac{k_{mn}}{k}\right)^2}\right\}$	0
$\beta k_{mn}>\lvert k\rvert$	$\frac{1}{\beta^2}\{kM-i\sqrt{\beta^2k^2_{mn}-k^2}\}$	0

s_{mn}	$x-x_0<0$
$\lvert k\rvert>k_{mn}$	$k\sqrt{1-\beta^2\left(\frac{k_{mn}}{k}\right)^2}$
$k_{mn}\geqslant\lvert k\rvert\geqslant\beta k_{mn}$	kM
$\beta k_{mn}>\lvert k\rvert$	$\frac{1}{2}\{kM-i\sqrt{\beta^2k^2_{mn}-k^2}\}$ $\quad\beta\equiv\sqrt{1-M^2}$

$$\Lambda_{mn}=\left(1-\frac{m^2}{k_{mn}^2R^2}\right)J_m^2(k_{mn}R)+\left\{\frac{dJ_m(r)}{dr}\right\}^2_{r=k_{mn}R} \tag{14}$$

and k_{mn} are the eigen values which satisfy

$$i\beta_w(k+\kappa_{mn}M)J_m(k_{mn}R)=-\left[\frac{dJ_m(r)}{dr}\right]_{r=k_{mn}R}. \tag{15}$$

As the usual way, substracting Eq. (11) multiplied by $P(\boldsymbol{r},\omega)$ from Eq. (6) multiplied by $G(\boldsymbol{r},\omega;\boldsymbol{r}_0,\omega_0)$ and integrating over the entire volume enclosed by the duct walls with interchanging $\boldsymbol{r}$ and $\boldsymbol{r}_0$ and using Eqs. (7) and (12) and the relation of the same x-dependence of $G(\boldsymbol{r};\boldsymbol{r}_0,\omega)$ and $P(\boldsymbol{r},\omega)$, one obtains

$$P(\boldsymbol{r},\omega)=\int \boldsymbol{F}(\boldsymbol{r}_0,\omega)\cdot\nabla_0G(\boldsymbol{r};\boldsymbol{r}_0,\omega)d\bar{r}_0. \tag{16}$$

Substituting Eq. (13) into Eq. (16) yields

$$P(\boldsymbol{r},\omega)=\frac{1}{i2\pi R^2}\sum_{m=-\infty}^{\infty}\sum_{n=0}^{\infty}\frac{1}{\Lambda_{mn}s_{mn}}J_m(k_{mn}r)\exp\{-i(m\theta+\kappa_{mn}x)\}$$
$$\cdot\int \boldsymbol{F}(\boldsymbol{r}_0,\omega)\cdot\nabla_0[J_m(k_{mn}r_0)\exp\{i(m\theta_0+\kappa_{mn}x_0)\}]d\boldsymbol{r}_0. \tag{17}$$

The acoustic source of a B-bladed rotor is now modelled by B point dipoles rotating at a constant angular velocity Ω around the x-axis in a plane $x_0=0$ at an effective radius $r_0=R_e$, having the strength $\boldsymbol{f}_\nu(t_0)$ for the ν-th dipole whose position is

$$\boldsymbol{a}_\nu(t_0)=(0,R_e,\Omega t_0+\theta_\nu)\qquad \nu=0,1,\cdots,B-1 \tag{18}$$

where θ_ν is the angular position of the ν-th blade at $t_0=0$. This approximation of

point dipole sources would be acceptable if the physical dimensinn of the source in question were of the order less than the wave length of the sound generated. The dipole strength distribution of the ν-th blade is then

$$\boldsymbol{f}_\nu(\boldsymbol{r}_0, t_0)=\boldsymbol{f}_\nu(t_0)\delta\{\boldsymbol{r}-\boldsymbol{a}_\nu(t_0)\}=\boldsymbol{f}_\nu(t_0)\delta(x_0)\delta(r_0-R_e)\delta(\theta_0-\Omega t-\theta_\nu)\frac{1}{r_0} \tag{19}$$

and the overall dipole strength is

$$\boldsymbol{F}(\boldsymbol{r}_0, \omega)=\frac{1}{2\pi}\int_{-\infty}^{\infty}\sum_{\nu=0}^{B-1}\boldsymbol{f}_\nu(t_0)\delta\{\boldsymbol{r}_0-\boldsymbol{a}_\nu(t_0)\}e^{-i\omega t_0}dt_0. \tag{20}$$

The force $\boldsymbol{f}_\nu(t_0)$ can be decomposed into axial, radial and circumferential components, $(f_{x\nu}, f_{r\nu}, f_{\theta\nu})$. From a practical point of view, the radical component may be neglected in comparison with other two components to result in

$$\boldsymbol{F}(\boldsymbol{r}_0, \omega)=\frac{1}{2\pi}\int_{-\infty}^{\infty}\sum_{\nu=0}^{B-1}\{f_{x\nu}(t), 0, f_{\theta\nu}(t_0)\}\cdot\delta\{\boldsymbol{r}_0-\boldsymbol{a}_\nu(t_0)\}e^{-i\omega t_0}dt_0. \tag{21}$$

Using Eq. (21) in Eq. (17), one obtains the sound pressure spectrum as

$$P(\boldsymbol{r}_0, \omega)=\frac{1}{(2\pi R)^2}\sum_{m=-\infty}^{\infty}\sum_{n=0}^{\infty}\sum_{\nu=0}^{\infty}\frac{1}{\Lambda_{mn}s_{mn}}J_m(k_{mn}r)\exp\{-i(m\theta+\kappa_{mn}x)\}$$
$$\cdot\iint_{-\infty}^{\infty}\left\{\kappa_{mn}f_{x\nu}(t_0)+\frac{m}{r_0}f_{\theta\nu}(t)\right\}J_m(k_{mn}r_0)\delta\{\boldsymbol{r}_0-\boldsymbol{a}_\nu(t_0)\exp\{i(m\theta_0+\kappa_{mn}x_0-\omega t_0)\}dt_0d\boldsymbol{r}_0$$

or in terms of the Fourier time-transform of force components as

$$P(\boldsymbol{r}, \omega)=\frac{1}{2\pi R^2}\sum_{m=-\infty}^{\infty}\sum_{n=0}^{\infty}\sum_{\nu=0}^{B-1}\frac{1}{\Lambda_{mn}s_{mn}}J_m(k_{mn}r)J_m(k_{mn}R_e)$$
$$\cdot\left\{\kappa_{mn}F_{x\nu}(\omega-m\Omega)+\frac{m}{R_e}F_{\theta\nu}(\omega-m\Omega)\right\}\exp\{-im(\theta-\theta_\nu)-i\kappa_{mn}x\} \tag{22}$$

where

$$F_{x\nu}(\omega-m\Omega)=\frac{1}{2\pi}\int_{-\infty}^{\infty}f_{x\nu}(t_0)e^{-i(\omega-m\Omega)t_0}dt_0$$
$$F_{\theta\nu}(\omega-m\Omega)=\frac{1}{2\pi}\int_{-\infty}^{\infty}f_{\theta\nu}(t_0)e^{-i(\omega-m\Omega)t_0}dt_0. \tag{23}$$

From Eq. (22), it is easily seen that the associated spectrum has, in principle, harmonics of the rotating speed of rotor, being affected by many modal contributions. The contribution from axial fluctuating force is modified by a factor of mode axial wave number, κ_{mn}, whereas the circumferenctial force has a multiplication factor m.

2.2 *Far-Field Radiation of Sound Pressure from the Open End of Duct*

As mentioned in Introduction, the acoustic modes from within the duct are assumed not to be coupled with each other at duct terminations due to reflection, and hence

the acoustic field at the duct exit explicitly determines its far-field radiation from the open end of the duct. The axial particle velocity for an infinite duct then acts as the normal velocity imparted to the exterior medium. The far-field spectrum of acoustic radiation from the open end of the duct can thus be estimated by using the Green's function for an infinite medium which has no boundaries in it except a simple monopole distribution in the duct exit plane.

If $V_x(\boldsymbol{r}, \omega)$ denotes the distribution of the frequency spectrum of axial particle velocity at the duct exit, the distribution of the strength of monopoles at the duct is given by $\rho V_x(\boldsymbol{r}, \omega) r dr d\theta$, and the resulting sound pressure spectrum at the far-field point $\boldsymbol{x}$ can be expressed as

$$P(\boldsymbol{x}, \omega)=\int_0^R \int_0^{2\pi} G_0(\boldsymbol{x}; \boldsymbol{r}, \omega) i\omega\rho V_x(\boldsymbol{r}, \omega) r dr d\theta, \tag{24}$$

where $G(\boldsymbol{x}; \boldsymbol{r}, \omega)$ is the Green's function for an infinite medium given by

$$G(\boldsymbol{x}; \boldsymbol{r}, \omega)=\frac{e^{-iks}}{4\pi S} \tag{25}$$

where S is the distance between points $\boldsymbol{x}$ and $\boldsymbol{r}$, expressed in a spherical coordinates $\boldsymbol{x}(|\boldsymbol{x}|, \Theta, \Phi)$ and $\boldsymbol{r}(0, r, \theta)$ as

$$S=\{|\boldsymbol{x}|^2-2r|\boldsymbol{x}| \sin\Phi \cos(\Theta-\theta)+r^2\}^{1/2}.$$

In the far field ($|\boldsymbol{x}| \gg r$) the following approximation can be made

$$G(\boldsymbol{x}; \boldsymbol{r}, \omega)=\frac{e^{-ik|\boldsymbol{x}|}}{4\pi|\boldsymbol{x}|} e^{ikr \sin\Phi \cos(\Theta-\theta)}. \tag{26}$$

The frequency spectrum of axial particle velocity at the duct exit is obtainable with equation of motion in the x-direction, Eq. (2),

$$a\rho\left(ik-M\frac{\partial}{\partial x}\right) V_x(\boldsymbol{r}, \omega)=-\frac{\partial P(\boldsymbol{r}, \omega)}{\partial x}.$$

Since $P(\boldsymbol{r}, \omega)$ and $V_x(\boldsymbol{r}, \omega)$ have the same x-dependence in the form of $\exp(-i\kappa_{mn}x)$, the above equation gives

$$V_x(\boldsymbol{r}, \omega)=-\frac{\kappa_{mn}}{a\rho(k+\kappa_{mn}M)} P(\boldsymbol{r}, \omega),$$

and the velocity spectrum at the duct exit $x=\pm l$ is

$$V_x(\boldsymbol{r}, \omega)=\frac{1}{2\pi R^2} \sum_{m=-\infty}^{\infty} \sum_{n=0}^{\infty} \sum_{\nu=0}^{B-1} \frac{\kappa_{mn}}{a\rho(k+\kappa_{mn}M)} \frac{J_m(k_{mn}R_e)}{\Lambda_{mn}s_{mn}} e^{\mp\kappa_{mn}l}$$
$$\cdot\left\{\kappa_{mn}F_{x\nu}(\omega-m\Omega)+\frac{m}{R_e}F_{\theta\nu}(\omega-m\Omega)\right\} J_m(\kappa_{mn}r) e^{-im(\theta-\theta_\nu)}. \tag{27}$$

Substituting Eqs. (26) and (27) into Eq. (24) yields

$$P(\boldsymbol{x},\omega)=\frac{e^{-ik|\boldsymbol{x}|}}{4\pi|\boldsymbol{x}|}\sum_{m=-\infty}^{\infty}\sum_{n=0}^{\infty}\sum_{\nu=0}^{B-1}\frac{1}{2\pi R^2}\frac{ik\kappa_{mn}}{k+\kappa_{mn}M}\frac{J_m(k_{mn}R_e)}{\Lambda_{mn}s_{mn}}$$
$$\cdot e^{\mp i\kappa_{mn}l}\left\{\kappa_{mn}F_{x\nu}(\omega-m\Omega)+\frac{m}{R_e}F_{\theta\nu}(\omega-m\Omega)\right\}$$
$$\cdot\int_0^R\int_0^{2\pi}rJ_m(k_{mn}r)\exp\{-im(\theta-\theta_\nu)+ikr\sin\Phi\cos(\theta-\Theta)\}d\theta dr, \quad (28)$$

where $\exp(\mp i\kappa_{mn}l)$ means that the left hand side of equation consists of a linear summation of the terms at $x=l$ and $x=-l$. If $M=0$, it implies $2\exp(-i\kappa_{mn}l)$. With the relations

$$\int_0^{2\pi}\exp\{i\alpha\cos(\theta-\Theta)-im(\theta-\Theta)\}d\theta=2\pi e^{im\pi/2}J_m(\alpha)$$
$$\int_0^R rJ_m(\alpha r)J_m(\beta r)dr=\frac{R}{\alpha^2-\beta^2}\{\beta J_m(\alpha R)J_{m-1}(\beta R)-\alpha J_{m-1}(\alpha R)J_m(\beta R)\}\quad(\alpha\neq\beta)$$

Eq. (28) can be rewritten as

$$P(\boldsymbol{x},\omega)=\frac{e^{-k|\boldsymbol{x}|}}{4\pi|\boldsymbol{x}|}\sum_{m=-\infty}^{\infty}\sum_{n=0}^{\infty}\sum_{\nu=0}^{B-1}\frac{1}{R}\frac{ik\kappa_{mn}}{k+\kappa_{mn}M}\frac{e^{\mp i\kappa_{mn}l}e^{-im(\Theta-\theta_\nu-\pi/2)}}{\Lambda_{mn}s_{mn}(k_{mn}^2-k^2\sin^2\Phi)}$$
$$\cdot\left\{\kappa_{mn}F_{x\nu}(\omega-m\Omega)+\frac{m}{R_e}F_{\theta\nu}(\omega-m\Omega)\right\}J_m(k_{mn}R_e)$$
$$\cdot\{k\sin\Phi J_m(k_{mn}R)J_{m-1}(kR\sin\Phi)-k_{mn}J_{m-1}(k_{mn}R)J_m(kR\sin\Phi)\} \quad (29)$$

or in a reduced form as

$$P(\boldsymbol{x},\omega)=\sum_{m=-\infty}^{\infty}\sum_{\nu=0}^{B-1}\{F_{x\nu}(\omega-m\Omega)P_{xm\nu}^{(D)}(\boldsymbol{x},\omega)+F_{\theta\nu}(\omega-m\Omega)P_{\theta m\nu}^{(D)}(\boldsymbol{x},\omega)\} \quad (30)$$

where

$$P_{xm\nu}^{(D)}(\boldsymbol{x},\omega)=\sum_{n=0}^{\infty}\kappa_{mn}P_{mn\nu}^{(D)}(\boldsymbol{x},\omega)$$

$$P_{\theta m\nu}^{(D)}(\boldsymbol{x},\omega)=\sum_{n=0}^{\infty}\frac{m}{R_e}P_{mn\nu}^{(D)}(\boldsymbol{x},\omega)$$

$$P_{mn\nu}^{(D)}(\boldsymbol{x},\omega)=\frac{e^{-ik|\boldsymbol{x}|}}{4\pi|\boldsymbol{x}|}\frac{1}{R}\frac{ik\kappa_{mn}}{k+\kappa_{mn}M}\frac{e^{\mp i\kappa_{mn}l}e^{-im(\Theta-\theta_\nu-\pi/2)}}{\Lambda_{mn}s_{mn}(k_{mn}^2-k^2\sin^2\Phi)}J_m(\kappa_{mn}R_e)$$
$$\cdot\{k\sin\Phi J_m(k_{mn}R)J_{m-1}(kR\sin\Phi)-k_{mn}J_{m-1}(k_{mn}R)J_m(kR\sin\Phi)\}.$$

The time-averaged power spectral density of sound pressure can be defined as the ensemble average of $P(\boldsymbol{x},\omega)P^*(\boldsymbol{x},\omega)$

$$S_p(\boldsymbol{x},\omega)=E\{P(\boldsymbol{x},\omega)P^*(\boldsymbol{x},\omega)\} \quad (31)$$

where superscript * means the complex conjugate. By Eq. (30), one obtains the power spectral density

$$S_p(\boldsymbol{x},\omega)=\sum_{m=-\infty}^{\infty}\sum_{\nu=0}^{B-1}\sum_{\nu'=0}^{B-1}[E\{F_{x\nu}(\omega-m\Omega)F^*_{x\nu'}(\omega-m\Omega)\}P^{(D)}_{xm\nu}(\boldsymbol{x},\omega)P^{(D)*}_{xm\nu}(\boldsymbol{x},\omega)$$
$$+E\{F_{x\nu}(\omega-m\Omega)F^*_{\theta\nu'}(\omega-m\Omega)\}P^{(D)}_{xm\nu}(\boldsymbol{x},\omega)P^{(D)*}_{\theta m\nu'}(\boldsymbol{x},\omega)$$
$$+E\{F_{\theta\nu}(\omega-m\Omega)F^*_{x\nu'}(\omega-m\Omega)\}P^{(D)}_{\theta m\nu}(\boldsymbol{x},\omega)P^{(D)*}_{xm\nu'}(\boldsymbol{x},\omega)$$
$$+E\{F_{\theta\nu}(\omega-m\Omega)F^*_{\theta\nu'}(\omega-m\Omega)\}P^{(D)}_{\theta m\nu}(\boldsymbol{x},\omega)P^{(D)*}_{\theta m\nu'}(\boldsymbol{x},\omega)]. \qquad (32)$$

The θ_ν-dependence of $P^{(D)}_{xm\nu}$ and $P^{(D)}_{\theta m\nu}$ is in the form of $\exp(-im\theta_\nu)$. The ν-th θ-position of equally-spaced blades is given by

$$\theta_\nu=2\pi\nu/B.$$

If the turbulent blade loading is not completely correlated for different blades, as for the case of circumferential small-scale turbulence or large-scale fan, the summations with respect to ν and ν' can be reduced to

$$\sum_{\nu=0}^{B-1}\sum_{\nu'=0}^{B-1}E\{F_\nu\cdot F^*_{\nu'}\}P^{(D)}_{m\nu}P^{(D)*}_{m\nu'}=\sum_{\nu=0}^{B-1}E\{F_\nu\cdot F^*_\nu\}P^{(D)}_{m\nu}P^{(D)*}_{m\nu}.$$

Further, when the blade has the same turbulent loading,

$$\sum_{\nu=0}^{B-1}E\{F_\nu\cdot F^*_\nu\}P^{(D)}_{m\nu}P^{(D)*}_{m\nu}=B\cdot E\{F\cdot F^*\}P^{(D)}_m P^{(D)*}_m.$$

The power spectrum is then expressed as

$$S_p(\boldsymbol{x},\omega)=B\sum_{\text{(non-correlated)}\ m=-\infty}^{\infty}[E\{F_x(\omega-m\Omega)F^*_x(\omega-m\Omega)\}P^{(D)}_{xm}(\boldsymbol{x},\omega)P^{(D)*}_{xm}(\boldsymbol{x},\omega)$$
$$+E\{F_x(\omega-m\Omega)F^*_\theta(\omega-m\Omega)\}P^{(D)}_{xm}(\boldsymbol{x},\omega)P^{(D)}_{\theta m}(\boldsymbol{x},\omega)$$
$$+E\{F_\theta(\omega-m\Omega)F^*_x(\omega-m\Omega)\}P^{(D)}_{\theta m}(\boldsymbol{x},m)P^{(D)*}_{xm}(\boldsymbol{x},\omega)$$
$$+E\{F_\theta(\omega-m\Omega)F^*_\theta(\omega-m\Omega)\}P^{(D)}_{\theta m}(\boldsymbol{x},\omega)P^{(D)*}_{\theta m}(\boldsymbol{x},\omega)], \qquad (33)$$

where

$$P^{(D)}_{xm}(\boldsymbol{x},\omega)=\sum_{n=0}^{\infty}\kappa_{mn}P^{(D)}_{nm}(\boldsymbol{x},\omega)$$

$$P^{(D)}_{\theta m}(\boldsymbol{x},\omega)=\sum_{n=0}^{\infty}\frac{m}{R_e}P^{(D)}_{mn}(\boldsymbol{x},\omega)$$

$$P^{(D)}_{mn}(\boldsymbol{x},\omega)=\frac{1}{4\pi|\boldsymbol{x}|R}\frac{k\kappa_{mn}}{k+\kappa_{mn}M}\frac{e^{\mp i\kappa_{mn}l}}{\Lambda_{mn}s_{mn}}\frac{J_m(k_{mn}R_e)J_m(k_{mn}R)}{k^2_{mn}-k^2\sin^2\Phi}$$
$$\cdot\left\{k\sin\Phi\cdot J_{m-1}(k\sin\Phi)-\left(\frac{m}{R}-i\beta_w(k+\kappa_{mn}M)\right)J_m(kR\sin\Phi)\right\}$$

where Eq. (15) is used for $J_{m-1}(k_{mn}R)$.

If the turbulent blade loading is uniformly correlated, as the case of the turbulence with large scale in the θ-direction or small scale fans, by using the rlation

$$\sum_{\nu=0}^{B-1}e^{im\theta_\nu}=\begin{cases}1 & m=nB\\ 0 & m\neq nB\end{cases}\qquad (n\text{: integer})$$

the ν and ν' summations of Eq. (32) can be reduced to

$$\sum_{\nu=0}^{B-1}\sum_{\nu'=1}^{B-1} E\{F_\nu F_{\nu'}^*\}P_{m\nu}^{(D)}P_{m\nu'}^{(D)*} = E\{FF^*\}\sum_{\nu=0}^{B-1}P_{m\nu}^{(D)}\sum_{\nu'=0}^{B-1}P_{m\nu'}^{(D)*}$$
$$= B^2\cdot E\{FF^*\}P_{nB}^{(D)}P_{nB}^{(D)*}.$$

The power spectrum in this case is then given by

$$\underset{\text{(correlated)}}{S_p(\boldsymbol{x},\omega)} = B^2\sum_{m=-\infty}^{\infty}[E\{F_x(\omega-mB\Omega)F_x^*(\omega-mB\Omega)P_{x,mB}^{(D)}(\boldsymbol{x},\omega)P_{x,mB}^{(D)*}(\boldsymbol{x},\omega)$$
$$+E\{F_x(\omega-mB\Omega)F_\theta^*(\omega-mB\Omega)P_{x,mB}^{(D)}(\boldsymbol{x},\omega)P_{\theta,mB}^{(D)*}(\boldsymbol{x},\omega)$$
$$+E\{F_\theta(\omega-mB\Omega)F_x^*(\omega-mB\Omega)P_{\theta,mB}^{(D)}(\boldsymbol{x},\omega)P_{x,mB}^{(D)*}(\boldsymbol{x},\omega)$$
$$+E\{F_\theta(\omega-mB\Omega)F_\theta^*(\omega-mB\Omega)P_{\theta,mB}^{(D)}(\boldsymbol{x},\omega)P_{\theta,mB}^{(D)*}(\boldsymbol{x},\omega)] \tag{34}$$

The power spectral density for circumferentially non-correlated turbulence has harmonics of the rotating frequency of rotor, $m\Omega$. In the case of correlated turbulence onto equally-spaced blades, these harmonics between blade-pass frequencies are to be canceled out each other, remaining only harmonics of blade-pass frequences.

3. Far-Field Acoustic Radiation by Random Rotor-Blade Loading in Free Space

To examine the features of the acoustic radiation caused by inlet-turbulence/rotor interaction in ducted space, it is convenient to deal with the same problem of fans operating in free space in the same way as used in the ducted case. With the model of rotating point dipole, the frequency spectrum of sound pressure by B-bladed rotor sources is given by Eq. (16) with the Green's function for an infinite medium Eq. (25),

$$P(\boldsymbol{x},\omega) = \int \boldsymbol{F}(\boldsymbol{r}_0,\omega)\cdot\nabla_0 G(\boldsymbol{x};\boldsymbol{r}_0,\omega)d\boldsymbol{r}_0 \tag{35}$$

where

$$G(\boldsymbol{x};\boldsymbol{r}_0,\omega) = \frac{e^{-ikS_0}}{4\pi S_0}.$$

The distance between points $\boldsymbol{x}$ and $\boldsymbol{r}_0$ is in the cylindrical ccordinates

$$S_0 = \{(x-x_0)^2 + r^2 + r_0^2 - 2rr_0\cos(\Theta-\theta_0)\}^{1/2}.$$

The frequency spectrum of dipole strength can be given by Eq. (21)

$$\boldsymbol{F}(\boldsymbol{r}_0,\omega) = \frac{1}{2\pi}\int_{-\infty}^{\infty}\sum_{\nu=1}^{B-1}\{f_{x\nu}(t_0),0,f_{\theta\nu}(t_0)\}\cdot\delta\{\boldsymbol{r}_0-\boldsymbol{a}_\nu(t_0)\}e^{-i\omega t_0}dt_0$$

where

$$\delta\{\boldsymbol{r}_0-\boldsymbol{a}_0(t)\} = \delta(x_0)\delta(r_0-R_e)\delta(\theta-\Omega t-\theta_\nu)\frac{1}{r_0}.$$

The frequency spectrum of far-field acoustic radiation from a B-bladed rotor in free-space is then given by

$$P(\boldsymbol{x},\omega)=\frac{1}{2\pi}\int_{-\infty}^{\infty}\sum_{\nu=0}^{B-1}\left(ik+\frac{1}{S}\right)\frac{e^{-ikS}}{4\pi S}\cdot\left\{\frac{x}{S}f_{x\nu}(t_0)+\frac{r}{S}\sin(\Theta-\Omega t_0-\theta_\nu)f_{\theta\nu}(t_0)\right\}e^{-i\omega t_0}dt_0 \tag{36}$$

where

$$\begin{aligned}S&=\{x^2+r^2+R_e^2-2rR_e\cos(\Theta-\Omega t_0-\theta_\nu)\}^{1/2}\\&=\{|\boldsymbol{x}|^2-2|\boldsymbol{x}|R_e\sin\Phi\cos(\Theta-\Omega t_0-\theta_\nu)+R_e^2\}^{1/2}.\end{aligned}$$

By taking the far-field approximation

$$ik+\frac{1}{S}\simeq ik$$

$$\frac{e^{-kS}}{S}\simeq\frac{e^{-ik|\boldsymbol{x}|}}{|\boldsymbol{x}|}e^{ikR_e\sin\Phi\cos(\Theta-\Omega t-\theta_\nu)},$$

Eq. (36) can be rewritten as

$$P(\boldsymbol{x},\omega)=\frac{1}{8\pi|\boldsymbol{x}|}\sum_{\nu=0}^{B-1}ike^{-ik|\boldsymbol{x}|}e^{ikR_e\sin\Phi\cos(\Theta-\Omega t-\theta_\nu)}\cdot\int_{-\infty}^{\infty}\{f_{x\nu}(t_0)\cos\Phi+f_{\theta\nu}(t_0)\sin\Phi\sin(\Theta-\Omega t_0-\theta_\nu)\}e^{-i\omega t_0}dt_0. \tag{36'}$$

Further, by using the relations

$$e^{i\alpha\cos\beta}=\sum_{m=-\infty}^{\infty}J_m(\alpha)e^{im(\beta+\pi/2)}$$

$$\sin\beta e^{i\alpha\cos\beta}=\sum_{m=-\infty}^{\infty}\frac{-m}{\alpha}J_m(\alpha)e^{im(\beta+\pi/2)},$$

Eq. (36)′ is reduced to

$$P(\boldsymbol{x},\omega)=\frac{e^{-ik|\boldsymbol{x}|}}{4\pi|\boldsymbol{x}|}\sum_{m=-\infty}^{\infty}\sum_{\nu=0}^{B-1}ike^{-im(\Theta-\theta_\nu-\pi/2)}\cdot J_m(kR_e\sin\Phi)\left\{\cos\Phi\cdot F_{x\nu}(\omega-m\Omega)+\frac{m}{kR_e}F_{\theta\nu}(\omega-m\Omega)\right\}, \tag{37}$$

where $F_{x\nu}(\omega-m\Omega)$ and $F_{\theta\nu}(\omega-m\Omega)$ are defined by Eq. (23). The similar expression of Eq. (37) as that of Eq. (30) is then

$$P(\boldsymbol{x},\omega)=\sum_{m=-\infty}^{\infty}\sum_{\nu=0}^{B-1}\{F_{x\nu}(\omega-m\Omega)P^{(F)}_{xm\nu}(\boldsymbol{x},\omega)+F_{\theta\nu}(\omega-m\Omega)P^{(F)}_{\theta m\nu}(\boldsymbol{x},\omega)\}, \tag{38}$$

where

$$P^{(F)}_{xm\nu}(\boldsymbol{x},\omega)=\cos\Phi\cdot P^{(F)}_{m\nu}(\boldsymbol{x},\omega)$$

$$P^{(F)}_{\theta m\nu}(\boldsymbol{x},\omega)=\frac{m}{kR_e}\cdot P^{(F)}_{m\nu}(\boldsymbol{x},\omega)$$

$$P^{(F)}_{m\nu}(\boldsymbol{x},\omega)=\frac{e^{-ik|\boldsymbol{x}|}}{4\pi|\boldsymbol{x}|}ike^{-ik(\Theta-\theta_\nu-\pi/2)}\cdot J_m(kR_e\sin\Phi).$$

The power spectral density of the sound pressure is thus given by

$$\begin{aligned}S_p(\boldsymbol{x},\omega)=\sum_{m=-\infty}^{\infty}\sum_{\nu=0}^{B-1}\sum_{\nu'=0}^{B-1}&[E\{F_{x\nu}(\omega-m\Omega)F^*_{x\nu'}(\omega-m\Omega)\}P^{(F)}_{xm\nu}(\boldsymbol{x},\omega)P^{(F)*}_{xm\nu'}(\boldsymbol{x},\omega)\\&+E\{F_{x\nu}(\omega-m\Omega)F^*_{\theta\nu'}(\omega-m\Omega)\}P^{(F)}_{xm\nu}(\boldsymbol{x},\omega)P^{(F)*}_{\theta m\nu'}(\boldsymbol{x},\omega)\\&+E\{F_{\theta\nu}(\omega-m\Omega)F^*_{x\nu'}(\omega-m\Omega)\}P^{(F)}_{\theta m\nu}(\boldsymbol{x},\omega)P^{(F)*}_{xm\nu'}(\boldsymbol{x},\omega)\\&+E\{F_{\theta\nu}(\omega-m\Omega)F^*_{\theta\nu'}(\omega-m\Omega)\}P^{(F)}_{\theta m\nu}(\boldsymbol{x},\omega)P^{(F)*}_{\theta m\nu'}(\boldsymbol{x},\omega)].\end{aligned}\tag{39}$$

Since the θ_ν-dependence of $P^{(F)}_{xm\nu}$ and $P^{(F)}_{\theta m\nu}$ is also in the form of $\exp(-im\theta_\nu)$, the power spectram can be expressed for circumferentially non-correlated and correlated turbulent blade-loadings of equally-spaced blades, respectively,

$$\begin{aligned}S_p(\boldsymbol{x},\omega)=_{\text{(non-correlated)}}B\sum_{m=-\infty}^{\infty}&[E\{F_x(\omega-m\Omega)F^*_x(\omega-m\Omega)\}P^{(F)}_{xm}(\boldsymbol{x},\omega)P^{(F)*}_{xm}(\boldsymbol{x},\omega)\\&+E\{F_x(\omega-m\Omega)F^*_\theta(\omega-m\Omega)\}P^{(F)}_{xm}(\boldsymbol{x},\omega)P^{(F)*}_{\theta m}(\boldsymbol{x},\omega)\\&+E\{F_\theta(\omega-m\Omega)F^*_x(\omega-m\Omega)\}P^{(F)}_{\theta m}(\boldsymbol{x},\omega)P^{(F)*}_{xm}(\boldsymbol{x},\omega)\\&+E\{F_\theta(\omega-m\Omega)F^*_\theta(\omega-m\Omega)\}P^{(F)}_{\theta m}(\boldsymbol{x},\omega)P^{(F)*}_{\theta m}(\boldsymbol{x},\omega)]\end{aligned}\tag{40}$$

$$\begin{aligned}S_p(\boldsymbol{x},\omega)=_{\text{(correlated)}}B^2\sum_{m=-\infty}^{\infty}&[E\{F_x(\omega-mB\Omega)F^*_x(\omega-mB\Omega)\}P^{(F)}_{x,mB}(\boldsymbol{x},\omega)P^{(F)*}_{x,mB}(\boldsymbol{x},\omega)\\&+E\{F_x(\omega-mB\Omega)F^*_\theta(\omega-mB\Omega)\}P^{(F)}_{x,mB}(\boldsymbol{x},\omega)P^{(F)*}_{\theta,mB}(\boldsymbol{x},\omega)\\&+E\{F_\theta(\omega-mB\Omega)F^*_x(\omega-mB\Omega)\}P^{(F)}_{\theta,mB}(\boldsymbol{x},\omega)P^{(F)*}_{x,mB}(\boldsymbol{x},\omega)\\&+E\{F_\theta(\omega-mB\Omega)F^*_\theta(\omega-mB\Omega)\}P^{(F)}_{\theta,mB}(\boldsymbol{x},\omega)P^{(F)*}_{\theta,mB}(\boldsymbol{x},\omega)]\end{aligned}\tag{41}$$

where

$$P^{(F)}_{xm}(\boldsymbol{x},\omega)=\cos\Phi P^{(F)}_m(\boldsymbol{x},\omega)$$

$$P^{(F)}_{\theta m}(\boldsymbol{x},\omega)=\frac{m}{kR_e}P^{(F)}_m(\boldsymbol{x},\omega)$$

$$P^{(F)}_m(\boldsymbol{x},\omega)=\frac{1}{4\pi|\boldsymbol{x}|}kJ_m(kR_e\sin\Phi).$$

The axial fluctuation component has the factor, $\cos\Phi$ (cf. κ_{mn} for the ducted-space), whereas the circumferential component has the same factor as for the ducted-space. The latter causes the directivity pattern consisting of m-lobes which is zero at $\Phi=0$. The former has the directivity of $\cos\Phi\cdot J_0(kR_e\sin\Phi)$, which means more radiation toward the axial direction. The additive and subtractive effect of these features leads to a flat, slightly asymmetric, overall directivity pattern.

4. Inlet-Turbulence and Random Rotor-Blade Loading

The inlet-turbulence is assumed to be statistically uniform over the entire rotor and convected in the axial direction by a uniform speed U. One of the most simple and useful models of atmospheric turbulence is the von Kármán model (Ref. 7). For axial and vertical components of turbulence, this model here applied results in the following spectral densities (Ref. 7)

$$E\{V_x(k_x)V_x(k_x)\}=\frac{\bar{v}_x^2\mathscr{L}_x}{\pi}\{1+(c_0\mathscr{L}_x k_x)^2\}^{-5/6}$$

$$E\{V_y(k_x)V_y(k_x)\}=\frac{\bar{v}_y^2\mathscr{L}_x}{\pi}\left\{1+\frac{8}{3}(c_0\mathscr{L}_x k_x)^2\right\}\{1+(c_x\mathscr{L}_x k)^2\}^{-11/6}$$

$$E\{V_x(k_x)V_y(k_x)\}=0$$

where $c_0=8.41$, $\bar{v}_x^2$ and $\bar{v}_y^2$ are the axial and vertical turbulence intensities, respectively, $\mathscr{L}_x$ the axial integral scale of turbulence, and k_x the axial wave number component. Since the turbulence is assumed to be convected in statistically frozen state at U, the axial wave number component k_x is related to the frequency ω by $k_x=\omega/U$. The power spectral density of inlet-turbulence in ω can then be given by

$$\begin{aligned}
E\{V_x(\omega)V_x(\omega)\}&=\frac{\bar{v}_x^2\mathscr{L}_x}{\pi U}\left\{1+\left(\frac{c_0\mathscr{L}_x}{U}\omega\right)^2\right\}^{-5/6}\\
E\{V_y(\omega)V_y(\omega)\}&=\frac{\bar{v}_y^2\mathscr{L}_x}{2\pi U}\left\{1+\frac{8}{3}\left(\frac{c_0\mathscr{L}_x}{U}\omega\right)^2\right\}\left\{1+\left(\frac{c_0\mathscr{L}_x}{U}\omega\right)^2\right\}^{-11/6}\\
E\{V_x(\omega)V_y(\omega)\}&=0.
\end{aligned}\tag{42}$$

The blade row is represented by a two-dimensional cascade of thin airfoils at a radius R_e. The blade deflection through the airfoil is assumed small, and the effects of compressibility of flow, the finite span of blade and all interference from neibouring blades are neglected. In such a case, the theory of Kemp and Sears (Ref. 8) gives the fluctuating response of the airfoil to the turbulent upwash component v_n. By this theory, the frequency spectrum of the random lift is

$$L(\omega)=\pi\rho cbV\cdot S(\bar{\omega})\cdot V_n(\bar{\omega}),\tag{43}$$

where c is the blade chord, b the span, $S(\bar{\omega})$ the Sears' function, $\bar{\omega}$ the reduced frequency

$$\bar{\omega}=\frac{c\omega}{2V},\tag{44}$$

V the steady relative flow velocity for a standing blade,

$$V=\{U^2+(R_e\Omega)^2\}^{1/2},\tag{45}$$

and $V_n(\bar{\omega})$ the frequency spectrum of turbulence velocity normal to V (Fig. 2).

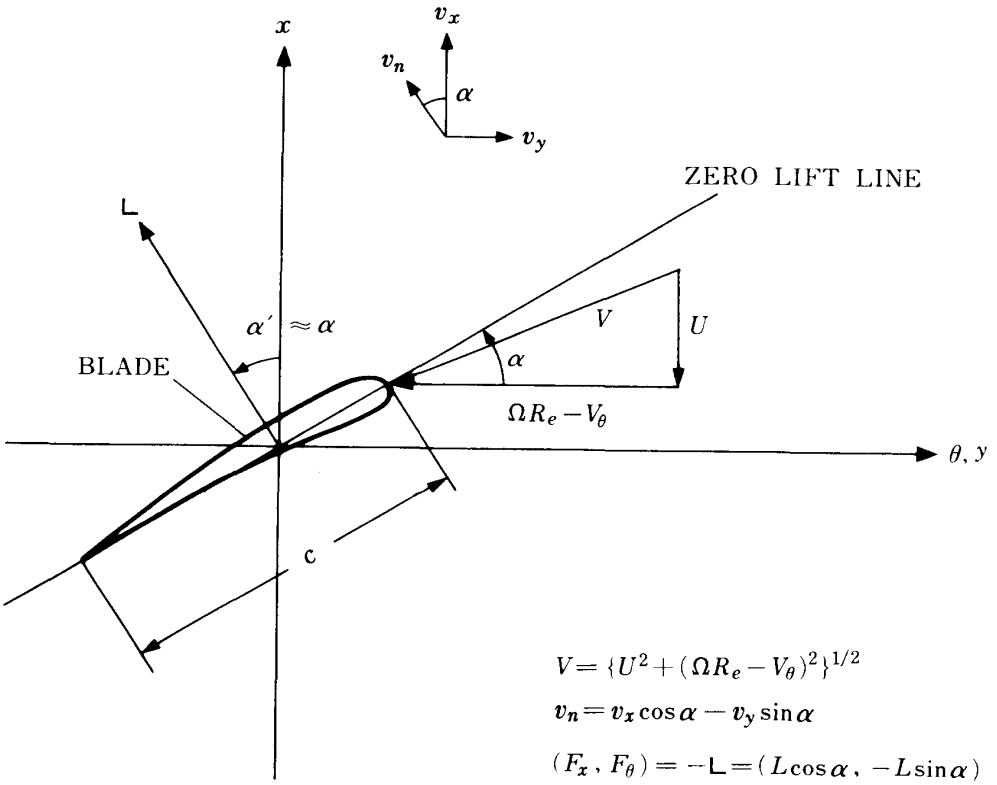

FIG. 2. Two dimensional airfoil in a uniform turbulent flow.

The lift response function $S(\bar{\omega})$ is given by

$$S(\bar{\omega}) = [i\bar{\omega}\{K_0(i\bar{\omega}) + K_1(i\bar{\omega})\}]^{-1} \tag{46}$$

where K is the modified Bessel function of the second kind. This particular form for $S(\bar{\omega})$ was given by Kemp (Ref. 9), and can be applied to the rotor blading provided there is a reasonable circumferential separation (Ref. 8). By the relation of Bessel functions

$$K_0(i\bar{\omega}) = -\frac{\pi}{2} i\{J_0(\bar{\omega}) - iY_0(\bar{\omega})\}$$

$$K_1(i\bar{\omega}) = -\frac{\pi}{2}\{J_1(\bar{\omega}) - iY_1(\bar{\omega})\},$$

the response function is written as

$$S(\bar{\omega}) = \left(\frac{\pi\bar{\omega}}{2}\right)^{-1}[J_0(\bar{\omega}) - Y_1(\bar{\omega}) - i\{Y_0(\bar{\omega}) + J_1(\bar{\omega})\}]^{-1}, \tag{47}$$

of which the power spectral density is then

$$S_e(\bar{\omega}) = E\{S(\bar{\omega})S^*(\bar{\omega})\} = \left(\frac{\pi\bar{\omega}}{2}\right)^{-2}[\{J_0(\bar{\omega}) - Y_1(\bar{\omega})\}^2 + \{Y_0(\bar{\omega}) + J_1(\bar{\omega})\}^2]^{-1}. \tag{48}$$

When the axial and azimuthal components of turbulence velocity are denoted by

v_x and v_y, respectively, $V_n(\omega)$ is then written as

$$V_n(\omega)=V_x(\omega)\cos\alpha-V_y(\omega)\sin\alpha, \tag{49}$$

where α is the angle of zero lift line from the rotating plane (Fig. 2) and

$$\begin{aligned} V_x(\omega)&=\frac{1}{2\pi}\int_{-\infty}^{\infty}v_x(t)e^{-i\omega t}dt \\ V_y(\omega)&=\frac{1}{2\pi}\int_{-\infty}^{\infty}v_y(t)e^{-i\omega t}dt. \end{aligned} \tag{50}$$

By neglecting drag force component, the force acting onto the medium is $(-L\cos\alpha, 0, L\sin\alpha)$ and hence the frequency spectra of random blade loading are

$$\begin{aligned} F_x(\omega)&=-L(\omega)\cos\alpha \\ F_\theta(\omega)&=L(\omega)\sin\alpha, \end{aligned} \tag{51}$$

which give

$$\begin{aligned} &E\{F_x(\omega)F_x^*(\omega)\}=E\{L(\omega)L^*(\omega)\}\cos^2\alpha \\ &E\{F_x(\omega)F_\theta^*(\omega)\}=E\{F_\theta(\omega)F_x^*(\omega)\}=-E\{L(\omega)L^*(\omega)\}\sin\alpha\cos\alpha \\ &E\{F_\theta(\omega)F_\theta^*(\omega)\}=E\{L(\omega)L^*(\omega)\}\sin^2\alpha. \end{aligned} \tag{52}$$

The power spectral density of random lift force is obtainable from Eqs. (43) and (49)

$$\begin{aligned} E\{L(\omega)L^*(\omega)\}=(\pi\rho cbV)^2[&E\{V_x(\omega)V_x^*(\omega)\}\cos^2\alpha \\ &-[E\{V_x(\omega)V_y^*(\omega)\}+E\{V_y(\omega)V_x^*(\omega)\}]\sin\alpha\cos\alpha \\ &+E\{V_y(\omega)V_y^*(\omega)\}\sin^2\alpha]S_e(\bar{\omega}). \end{aligned} \tag{53}$$

Substituting Eq. (42) into (53) yields

$$\begin{aligned} S_L(\omega)&=E\{L(\omega)L^*(\omega)\} \\ &=(\pi\rho cbV)S_e(\bar{\omega})\left[\frac{\bar{v}_x^2\mathscr{L}_x}{\pi U}\left\{1+\left(\frac{c_0\mathscr{L}_x}{U}\omega\right)^2\right\}^{-5/6}\cos^2\alpha\right. \\ &\left.+\frac{\bar{v}_y^2\mathscr{L}_x}{2\pi U}\left\{1+\frac{8}{3}\left(\frac{c_0\mathscr{L}_x}{U}\omega\right)^2\right\}\left\{1+\left(\frac{c_0\mathscr{L}_x}{U}\omega\right)^2\right\}^{-11/6}\sin^2\alpha\right] \end{aligned} \tag{54}$$

5. Frequency Spectra of Acoustic Radiation

With the random blade loading given by Eqs. (52) and (54), the frequency spectra of acoustic radiation associated with inlet-turbulence/rotor interaction are expressed with Eqs. (33), (34), (40) and (41) as follows;

Ducted space

$$S_{p\,(\text{non-correlated})}^{(D)}(\boldsymbol{x},\omega)=B\sum_{m=-\infty}^{\infty}S_L(\omega-m\Omega)\left|\sum_{n=0}^{\infty}\left(\kappa_{mn}\cos\alpha-\frac{m}{R_e}\sin\alpha\right)P_{mn}^{(D)}(\boldsymbol{x},\omega)\right|^2 \tag{55}_1$$

$$S^{(D)}_{\text{(correlated)}}(\boldsymbol{x},\omega)=B^2\sum_{m=-\infty}^{\infty}S_L(\omega-mB\Omega)\left|\sum_{n=0}^{\infty}\left(\kappa_{mB,n}\cos\alpha-\frac{mB}{R_e}\sin\alpha\right)P^{(D)}_{mB,n}(\boldsymbol{x},\omega)\right|^2 \quad (55)_2$$

Free space

$$S^{(F)}_{p\,\text{(non-correlated)}}(\boldsymbol{x},\omega)=B\sum_{m=-\infty}^{\infty}S_L(\omega-m\Omega)\left|\left(\cos\Phi\cos\alpha-\frac{m}{\omega R_e}\sin\alpha\right)P^{(F)}_{m}(\boldsymbol{x},\omega)\right|^2 \quad (56)_1$$

$$S^{(F)}_{p\,\text{(correlated)}}(\boldsymbol{x},\omega)=B^2\sum_{m=-\infty}^{\infty}S_L(\omega-mB\Omega)\left|\left(\cos\Phi\cos\alpha-\frac{mB}{\omega R_e}\sin\alpha\right)P^{(F)}_{mB}(\boldsymbol{x},\omega)\right|^2 \quad (56)_2$$

If the length scale is nondimensionalized by the duct radius R and the frequency spectra as

$$\bar{S}_p(\boldsymbol{x},\omega)=\frac{S_p(\boldsymbol{x},\omega)}{(\pi\rho cbV)^2(\bar{v}_x^2\mathscr{L}_x/\pi U)(1/R^2)(1/4\pi|\boldsymbol{x}|^2}, \quad (57)$$

$S_L(\omega)$, $P^{(D)}_{mn}(\boldsymbol{x},\omega)$ and $P^{(F)}_{mn}(\boldsymbol{x},\omega)$ are written as

$$S_L(\omega)=S_e(\omega)\left\{S_{vx}(\omega)\cos^2\alpha+S_{vy}(\omega)\frac{\bar{v}_y^2}{2\bar{v}_x^2}\sin^2\alpha\right\} \quad (58)$$

$$S_e(\omega)=(c_s\omega)^{-2}[\{J_0(c_s\omega)-Y_1(c_s\omega)\}^2+\{J_1(c_s\omega)+Y_0(c_s\omega)\}^2] \quad (59)$$

$$\left.\begin{aligned}S_{vx}(\omega)&=\{1+(c_t\omega)^2\}^{-5/6}\\ S_{vy}(\omega)&=\left\{1+\frac{8}{3}(c_t\omega)^2\right\}\{1+(c_t\omega)^2\}^{-11/6}\end{aligned}\right\} \quad (60)$$

$$c_s\equiv\frac{c}{2R}\frac{a}{V}\qquad c_t\equiv c_0\frac{a}{U}\frac{\mathscr{L}_x}{R}$$

$$P^{(D)}_{mn}(\boldsymbol{x},\omega)=\frac{\omega\kappa_{mn}}{\omega+\kappa_{mn}M}\frac{e^{\mp i\kappa_{mn}l}}{\Lambda_{mn}s_{mn}}\frac{J_m(k_{mn}R_e)J_m(k_{mn})}{k_{mn}^2-\omega^2\sin^2\Phi}$$
$$\cdot[\omega\sin\Phi\cdot J_{m-1}(\omega\sin\Phi)-\{m-i\beta_w(\omega+\kappa_{mn}M)\}J_m(\omega\sin\Phi)] \quad (61)$$

$$P^{(F)}_{mn}(\boldsymbol{x},\omega)=\omega J_m(\omega R_e\sin\Phi) \quad (62)$$

where ω, Ω and R_e mean

$$kR=\frac{\omega R}{a}\to\omega\qquad\frac{\Omega R}{a}\to\Omega\qquad\frac{R_e}{R}\to R_e.$$

In the expression of Eqs. (55), the term of $|\ \ |^2$ has the contribution from both inlet and outlet open ends, hence it can be written in the form

$$\left|\sum_{n=0}^{\infty}\left(\kappa_{mn}\cos\alpha-\frac{m}{R_e}\sin\alpha\right)P^{(D)}_{mn}(\boldsymbol{x},\omega)\right|^2$$
$$=\left|\sum_{n=0}^{\infty}\left\{(\kappa^+_{mn}P^+_{mn}+\kappa^-_{mn}P^-_{mn})\cos\alpha-\frac{m}{R_e}P^{+l}_{mn}+P^{-l}_{mn})\sin\alpha\right\}\right|^2\equiv A^{(D)}_m(\omega)$$

where

$$\kappa^{+}_{mn}=(\kappa_{mn})_{x=+l} \qquad \kappa^{-}_{mn}=(\kappa_{mn})_{x=-l}$$
$$P^{+}_{mn}=\{P^{(D)}_{mn}\}_{x=+l} \qquad P^{-}_{mn}=\{P^{(D)}_{mn}\}_{x=-l}.$$

Further, the spectra can be expressed in one-side frequency ($\omega>0$) as

$$\underset{\text{(non-correlated)}}{\bar{S}_p(\boldsymbol{x},\omega)}=BS_L(\omega)A_0(\omega)+A_0(-\omega)\}$$
$$+B\sum_{m=1}^{\infty}[S_L(\omega+m\Omega)\{A_m(\omega)+A_{-m}(-\omega)\}$$
$$+S_L(\omega-m\Omega)\{A_{-m}(\omega)+A_m(-\omega)\}] \tag{63}$$

$$\underset{\text{(correlated)}}{\bar{S}_p(\boldsymbol{x},\omega)}=B^2S_L(\omega)\{A_0(\omega)+A_0(-\omega)\}$$
$$+B^2\sum_{m=1}^{\infty}[S_L(\omega+mB\Omega)\{A_{mB}(\omega)+A_{-mB}(-\omega)\}$$
$$+S_L(\omega-mB\Omega)\{A_{-mB}(\omega)+A_{mB}(-\omega)\}] \tag{64}$$

where $A_m(\omega)$ means the term $|\quad|^2$ in Eqs. (55) and (56).

6. Numerical Results and Discussions

To show the features of the far-field acoustic radiation caused by inlet-turbulence/rotor interaction, Eqs. (63) and (64) are numerically computed for a fan with parameters shown in Table 2. The associated spectra consist of complicated modal contributions so that sufficiently fine mesh size of frequency is required for the computation of spectral density. For the purpose of computational economy, the aerodynamic response function, Eq. (48), is approximated by a following simple function (Appendix B), of which the degree of approximation is illustrated in Fig. 3.

Table 2. Parameters

Parameters			
Effective radius R_e/R		0.8	
Blade span R/c		3	
Blade angle α^0	30	45*	60
Wall admittance β_w		0	
Turbulence intensity $\overline{v_\theta}^2/\overline{v_x}^2$		1	
Turbulence scale $\mathscr{L}_x/R$	0.1	1*	10
Duct length l/R	0.1	1*	10
Roter speed $\Omega R_e/a$	0.3	0.5*	0.7
Flow velocity U/a	0**	0.3	0.5
Blade number B	4		8

* Standard values which are used otherwise not stated.

** For cases of $U/a=0$ and free space, U/a in Eq. (45) for V/a is 0.5.

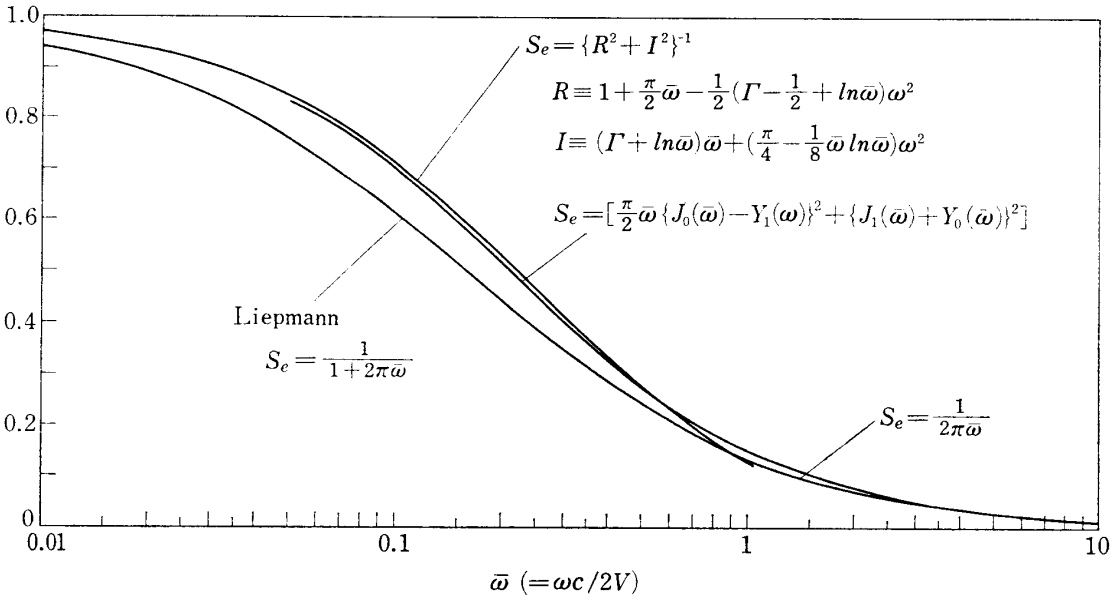

FIG. 3. Sears function and its approximation.

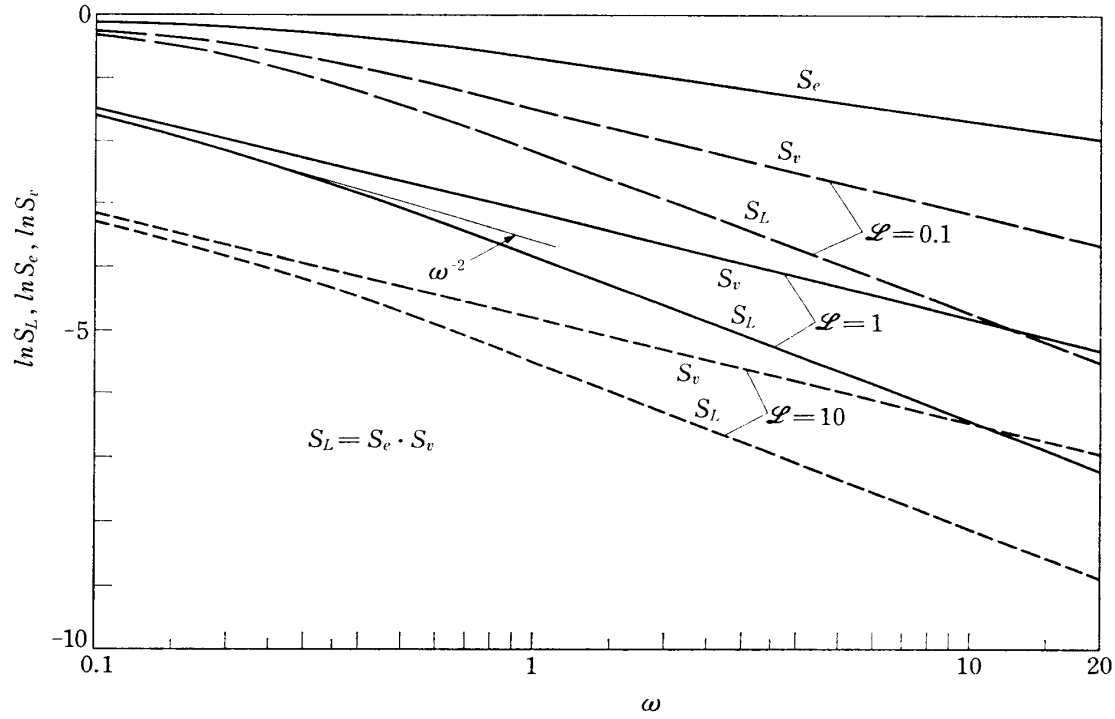

FIG. 4. Power spectral density of fluctuating lift, $S_L(\omega)$.

$$S_e(\bar{\omega})=\left[\left\{1+\frac{\pi}{2}\bar{\omega}-\frac{1}{2}\left(\Gamma-\frac{1}{2}+\ln\bar{\omega}\right)\bar{\omega}^2\right\}^2+\left\{(\Gamma+\ln\bar{\omega})\bar{\omega}+\left(\frac{\pi}{4}-\frac{1}{8}\bar{\omega}\ln\bar{\omega}\right)\bar{\omega}^2\right\}^2\right]^{-1} \qquad (\bar{\omega}<0.9)$$

$$=\frac{1}{2\pi\bar{\omega}} \qquad (\bar{\omega}\geqslant 0.9)$$

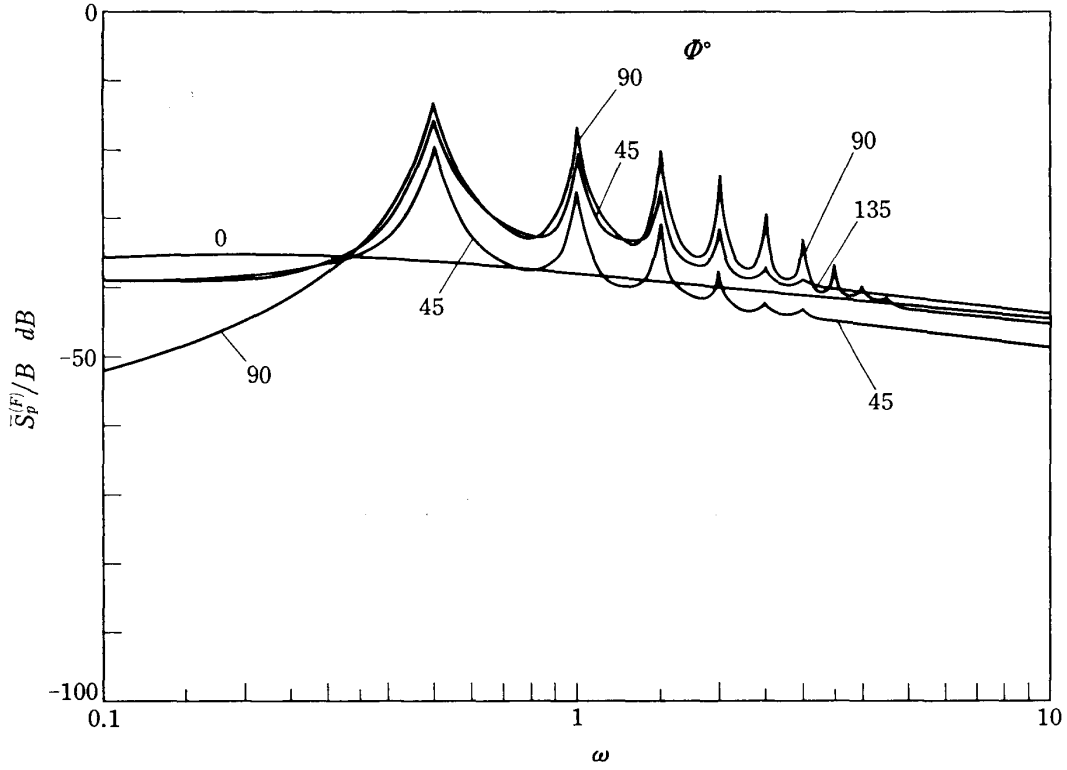

(a) Non-correlated turbulence.

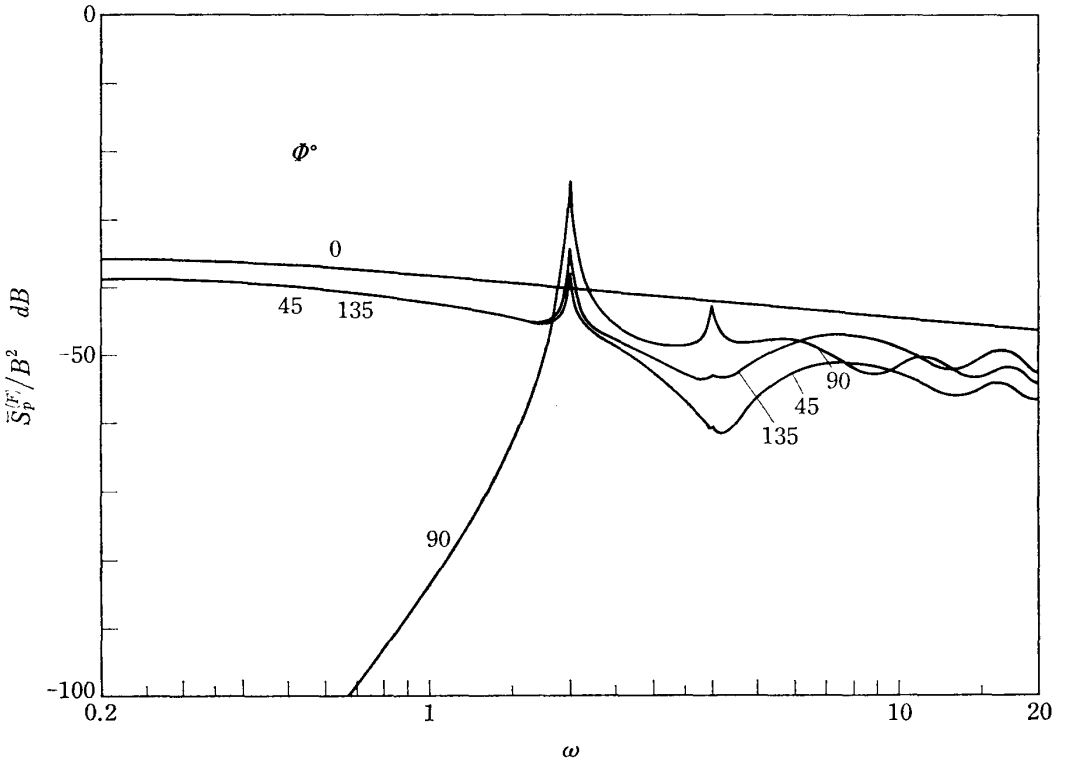

(b) Correlated turbulence, $B=4$.

FIG. 5. Frequency spectra of free-space fan noise.

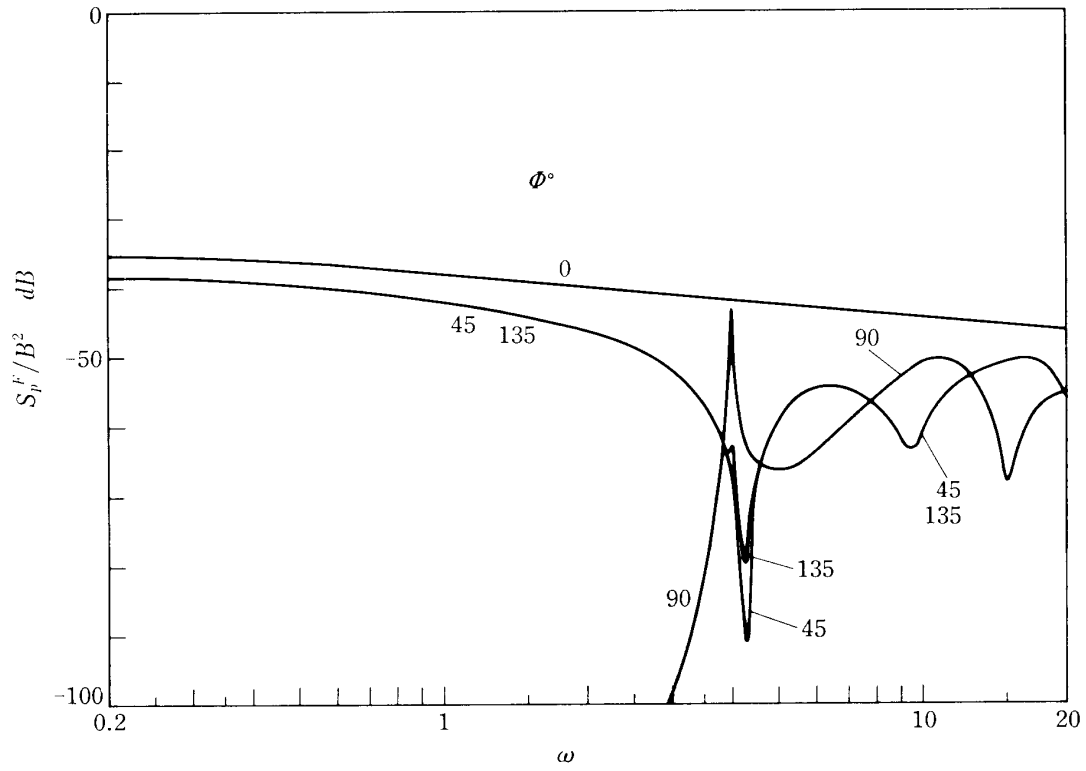

(c) Correlated turbulence, $B=8$.

FIG. 5. Frequency spectra of free-space fan noise.

Examples of lift response to von Kármán turbulence with this aerodynamic response function, Eq. (54), are shown in Fig. 4.

Free-space case

Figures 5 to 8 shows the frequency spectra for the free-space case. As seen in Fig. 5(a), the spectrum for non-correlated turbulence has peaks at harmonic frequencies of the rotor-speed. Correlated turbulence exicits harmonics of the blade-pass frequency, $mB\Omega$.

In the plane of rotor-rotating ($\Phi=90°$), the thrust component of random lift fluctuation makes no contribution to the acoustic radiation, which is solely dominated by the torque component;

$$\bar{S}_p^{(F)}(\Phi=90°,\omega)\sim\sum_m S_L(\omega\pm m\Omega)\left\{\frac{m}{R_e}\sin\alpha\cdot J_m(\omega R_e)\right\}^2$$

At the neighborhood of the peak frequency ($\omega\simeq m\Omega$), since $S_L\sim\omega^{\pm(2\sim3)}$, the spectral density behaves like

$$\bar{S}_p^{(F)}(\Phi=90°,\omega\simeq m\Omega)\sim\begin{cases}\omega^{2\sim3}J_m^2(\omega R_e) & \omega\lesssim m\Omega\\ \omega^{-(2\sim3)}J_m^2(\omega R_e) & \omega\gtrsim m\Omega\end{cases}$$

The peak values of harmonics are

$$\bar{S}_p^{(F)}(\Phi=90°,\omega=m\Omega)\sim\{mJ_m(m\Omega R_e)\}^2.$$

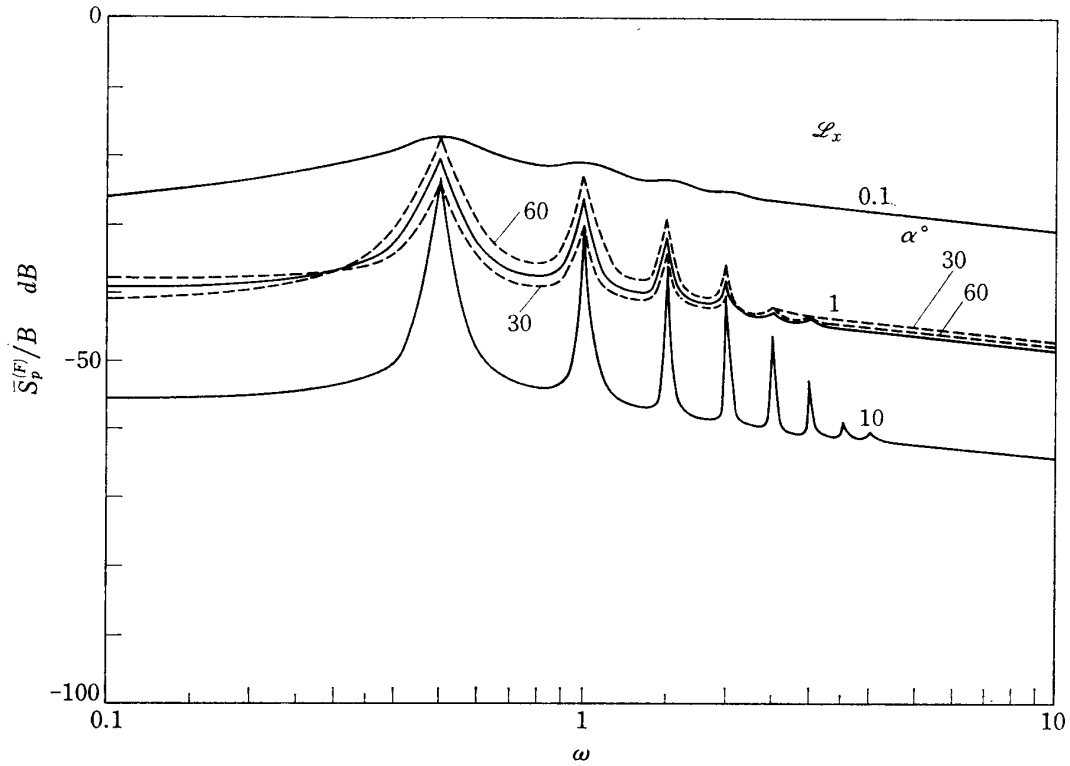

(a) Non-correlated turbulence.

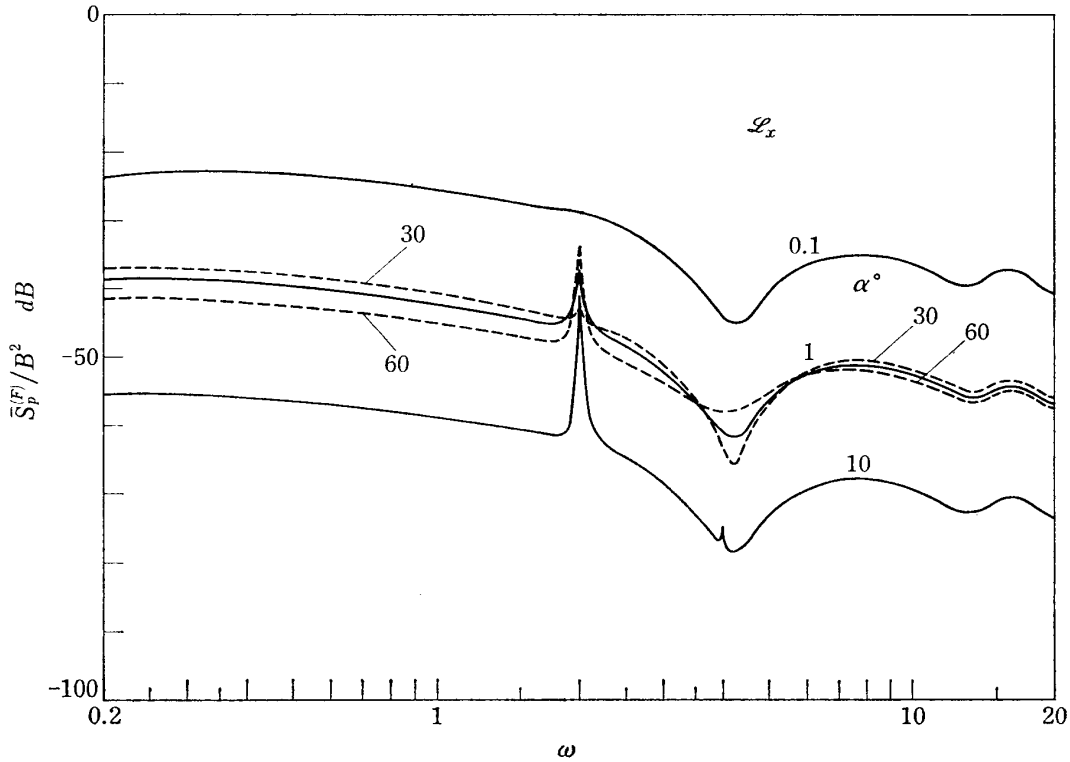

Correlated turbulence, $B=4$.

FIG. 6. Effect of turbulence scale in free space; $\Phi=45°$.

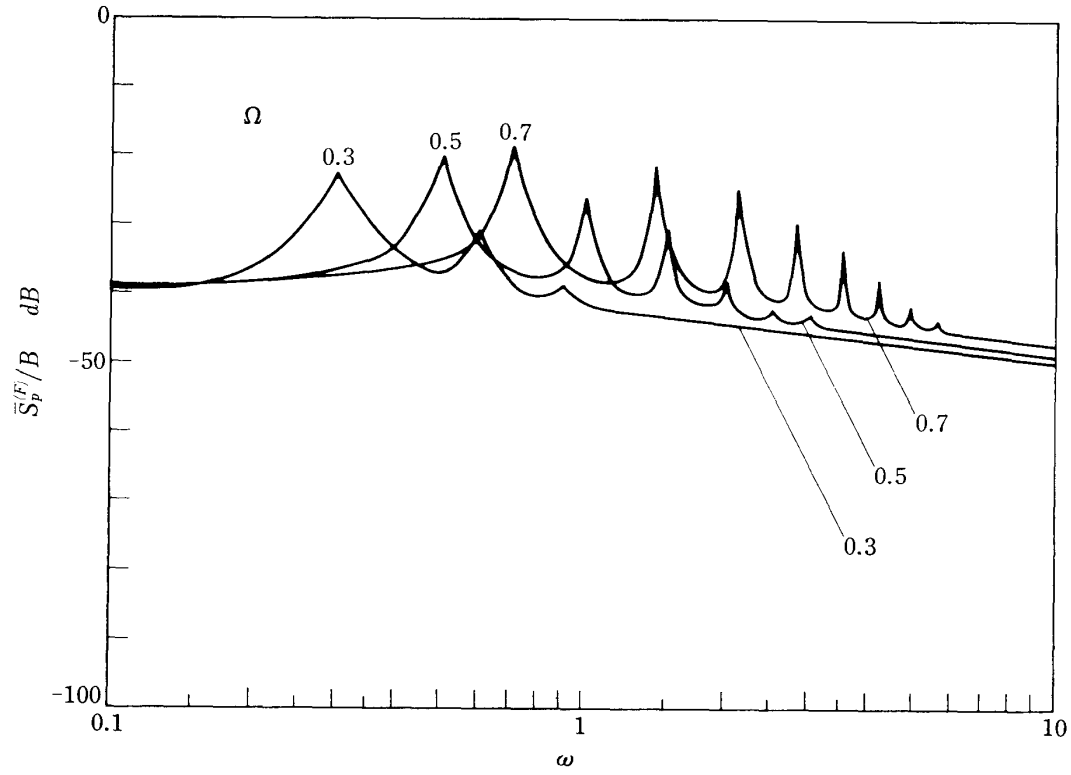

(a) Non-correlated, turbulence.

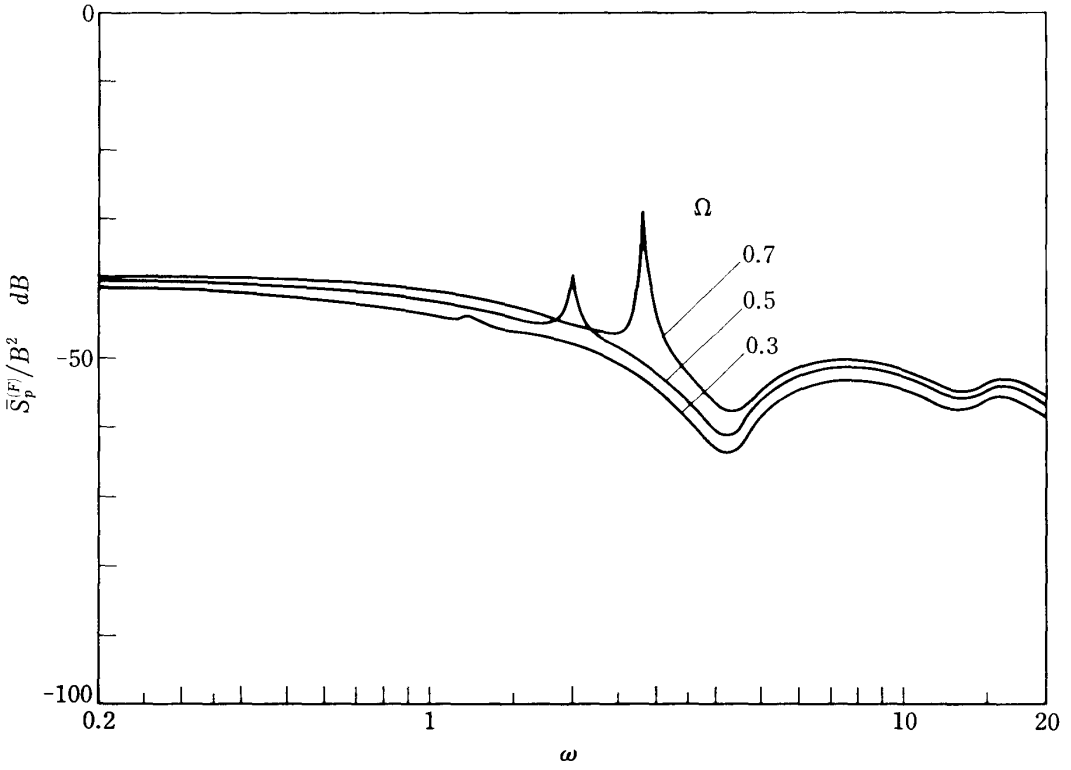

(b) Correlated turbulence, $B=4$.

FIG. 7. Effect of rotor speed in free space; $\Phi=45°$.

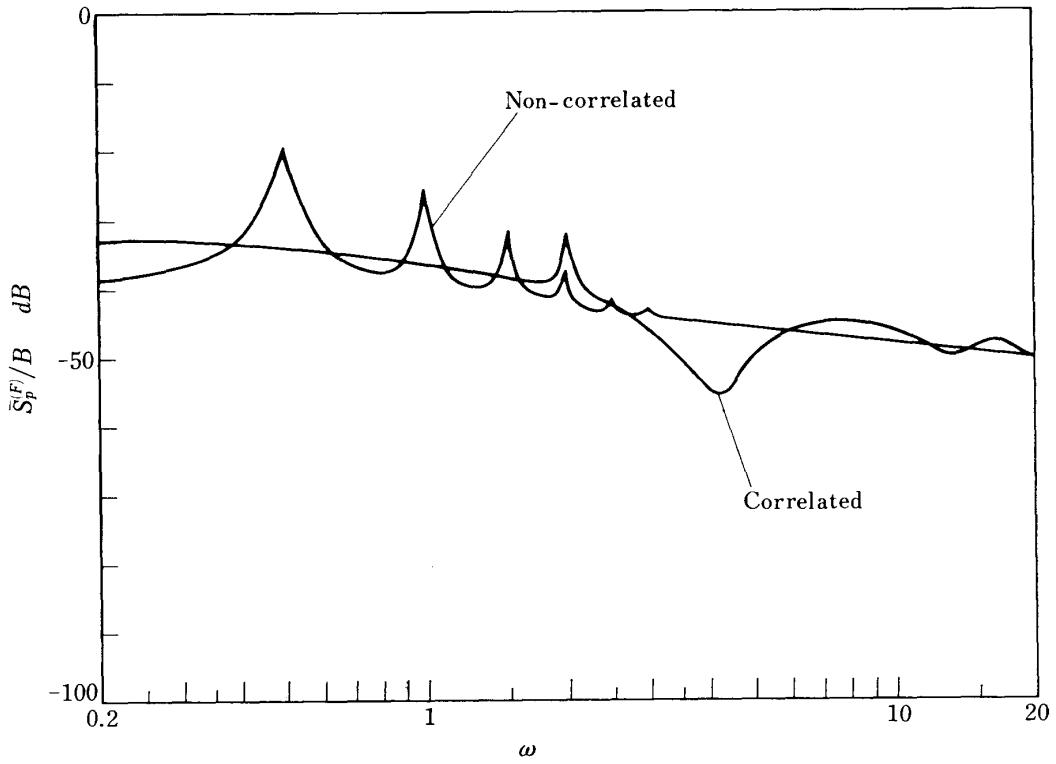

(a) $\Phi=45°$.

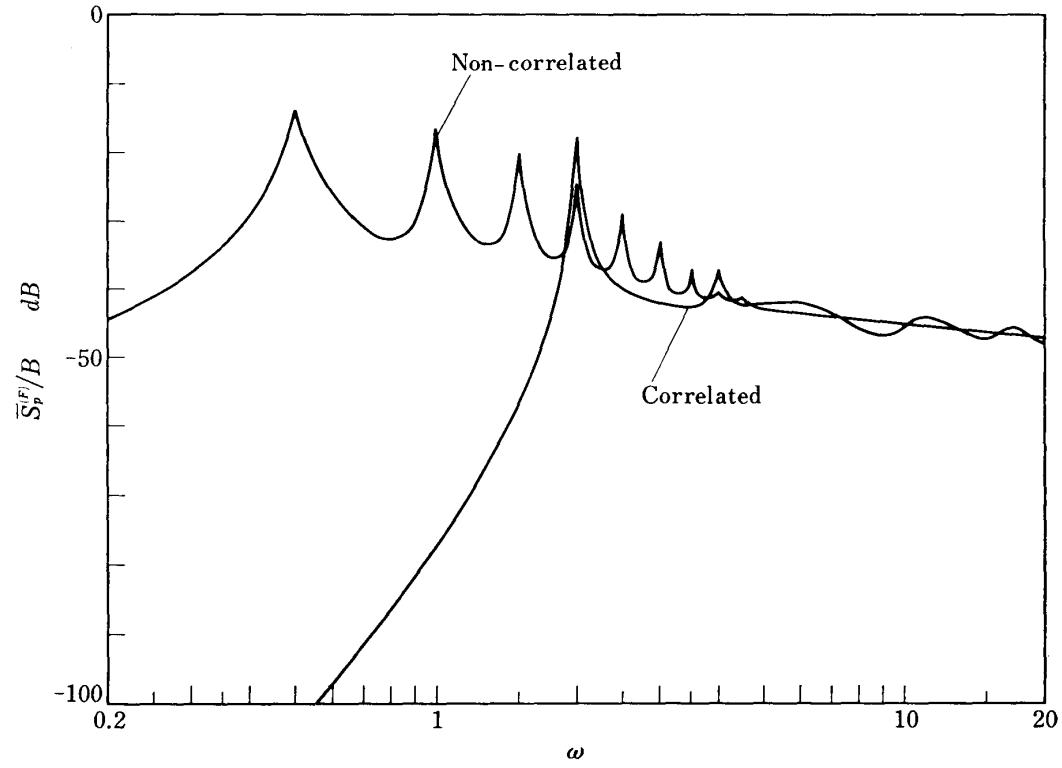

(b) $\Phi=90°$.

FIG. 8. Effect of turbulence correlation in free space; $B=4$.

At $\Phi=45°$, the thrust component comes into contribution mainly through the term of $J_0(\omega R_e \sin\Phi)$ which increases lower frequency components of spectrum. At lower frequencies, since $S_L \sim \omega^{-(2\sim3)}$ and $J_0 \sim 1$, $\bar{S}_p^{(F)}$ becomes proportional to $\omega^{0\sim1}$. The dips at $\omega=4.25$ in Figs. 5(b) and (c) correspond to the first zero of $J_0(\omega R_e \sin\Phi)$. The peak values of harmonics are given by

$$\bar{S}_p^{(F)}(\Phi=45°, \omega=m\Omega) \sim \left\{\left(\frac{m\Omega}{\sqrt{2}}\cos\alpha - \frac{m}{R_e}\sin\alpha\right)J_m\left(\frac{m\Omega R_e}{\sqrt{2}}\right)\right\}^2$$

which is always smaller than the corresponding peak value for $\Phi=90°$.

In the axial direction, only the J_0 term determines the acoustic radiation. The spectral density is then roughly proportional to $\omega^{0\sim-1}$, since $S_L \sim \omega^{-(2\sim3)}$ and $J_0(0)=1$.

As shown in Fig. 6, the axial scale of turbulence has an effect to make the spectrum less wavy, by broadening the band width of peaked spectral density. Although the nondimensional $\bar{S}_p$ is shifted upward with smaller scale of turbulence due to the behavior of lift response (see Fig. 4), the absolute value of the dimensional $S_p(\sim \mathscr{L}\bar{S}_p)$

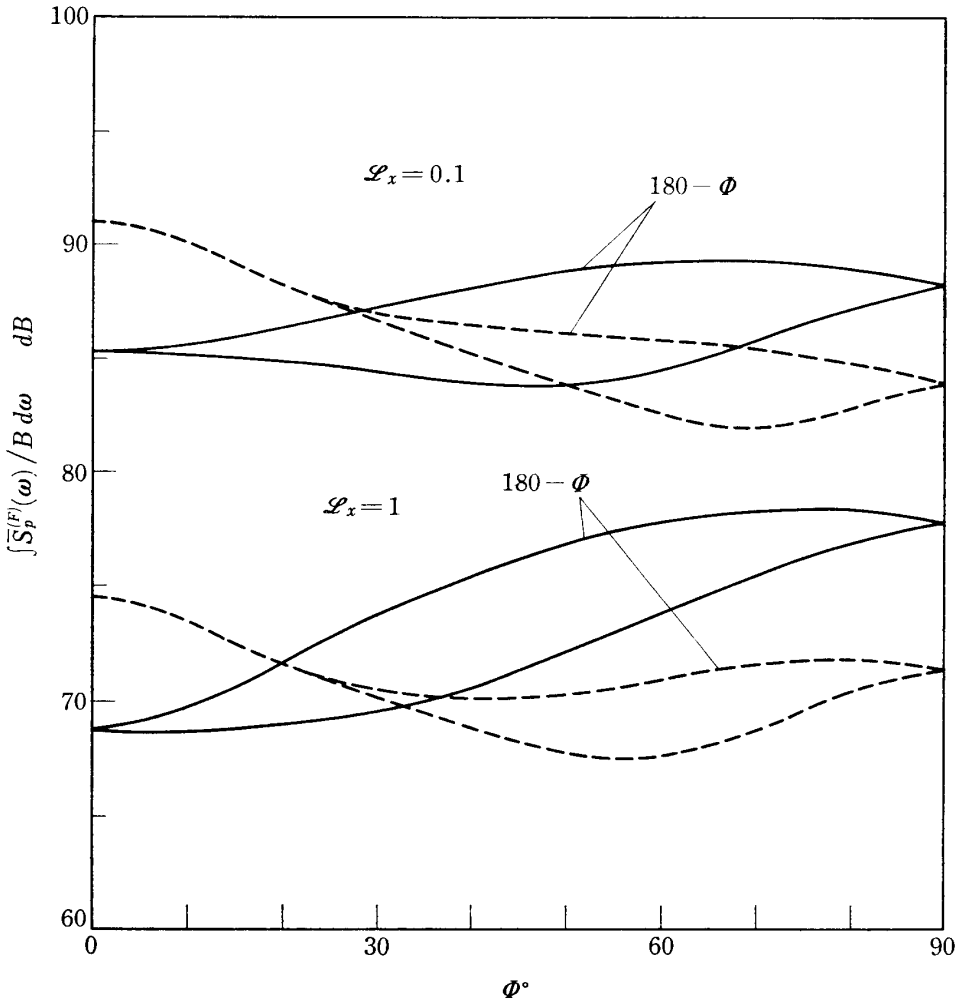

FIG. 9. Directivity of sound pressure in free space;
— non-correlated turbulence, ---- correlated turbulence.

may be less affected by the axial scale of turbulence. As shown in Fig. 6, the blade angle has little effect on the spectrum.

The effect of rotational speed of the rotor is shown in Fig. 7, which has more peaks at $\omega=m\Omega$ or $\omega=mB\Omega$ with increasing Ω. Figure 8 shows the comparison of effects of non-correlated and correlated turbulence. As mentioned before, for the correlated turbulence, the harmonics of the rotor-speed between blade-pass harmonics, $\omega=(mB+1)\Omega, (mB+2)\Omega, \cdots, (mB+B-1)\Omega$ are correlated to be canceled out.

Figure 9 shows the directivity of the far-field acoustic radiation, which is integrated the spectral density with respect to frequency. The sound pressure radiated close to the axial direction ($\Phi=0$) is controlled by the thrust component of fluctuating lift through the J_0 term. The radiation toward the rotor plane ($\Phi=90°$) is much contributed from the torque component characterized by the J_m term ($m\geqslant 1$). The additive effect of these two components makes the directivity almost flatten, although the difference of the effects at forward and downward directions results in slightly asymmetric directivity pattern. In the case of non-correlated turbulence, the contribution from large number of harmonics increases the radial radiation.

Ducted-space case

The frequency spectra for the ducted-space case are shown in Figs. 10 to 14 are for the case without mean flow in duct ($M=0$), and Figs. 15 to 19 for the case with mean flow ($M\neq 0$). In the ducted-space case, the most remarkable features of frequency spectrum come from the characteristics of duct cut-off modes. In these figures, decaying modes are also taken into account for the source distribution at

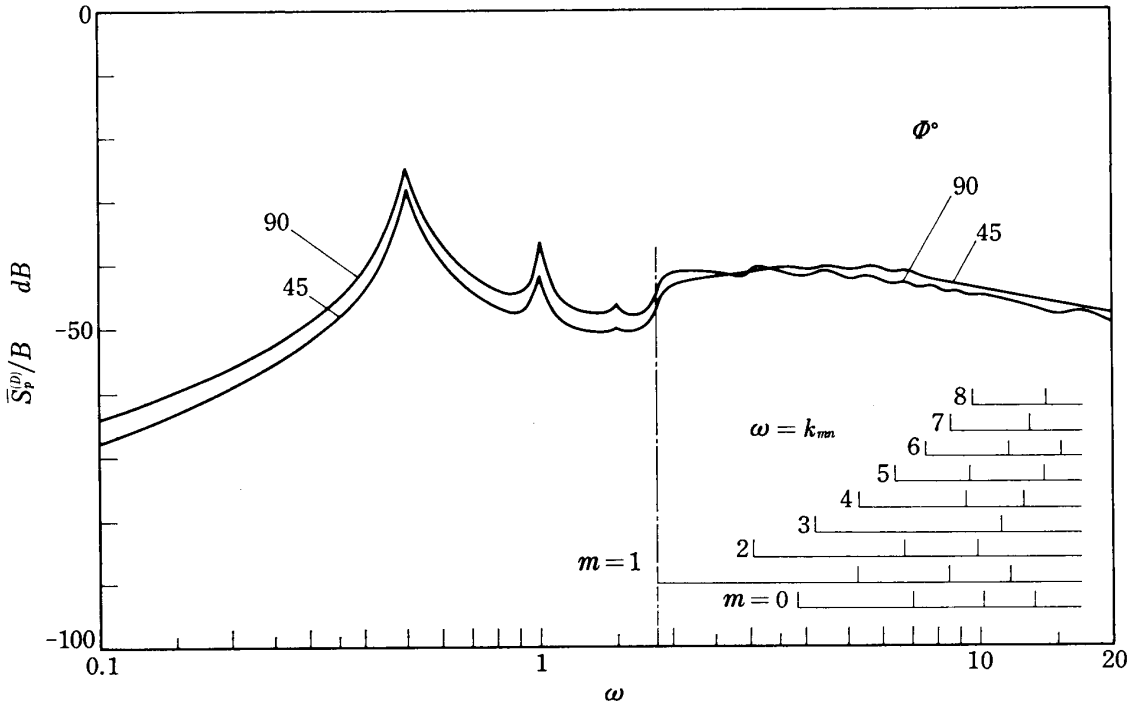

(a) Non-correlated turbulence.

FIG. 10. Frequency spectra of ducted-space fan noise without mean flow; $M=0$.

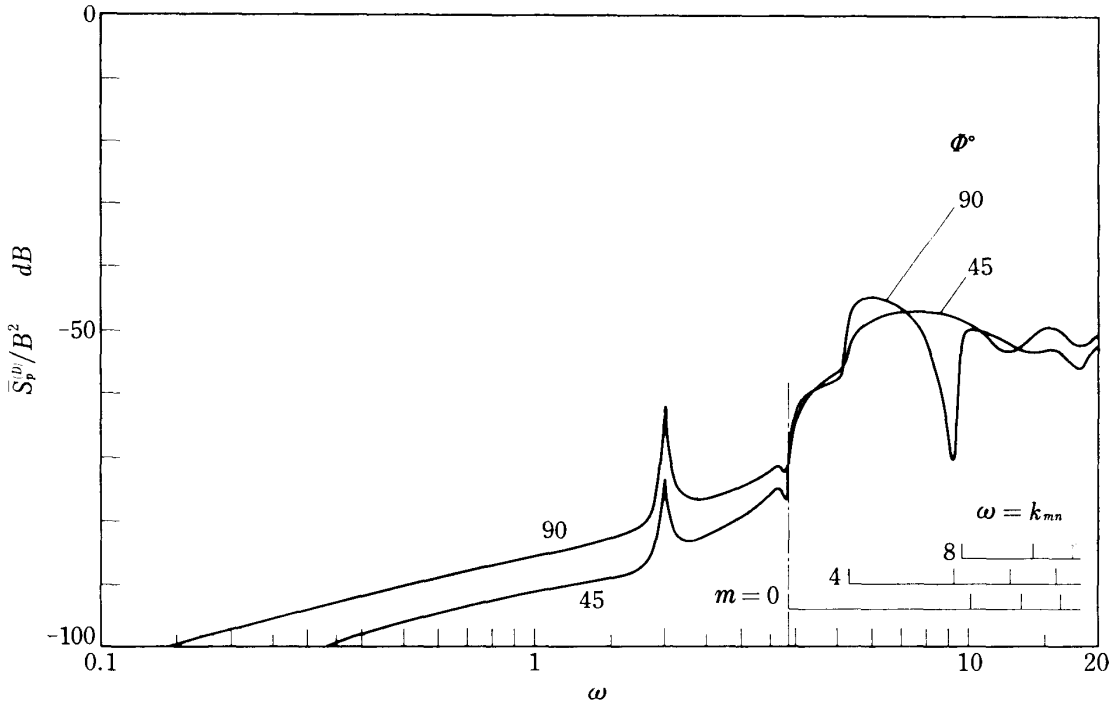

(b) Correlated turbulence, $B=4$.

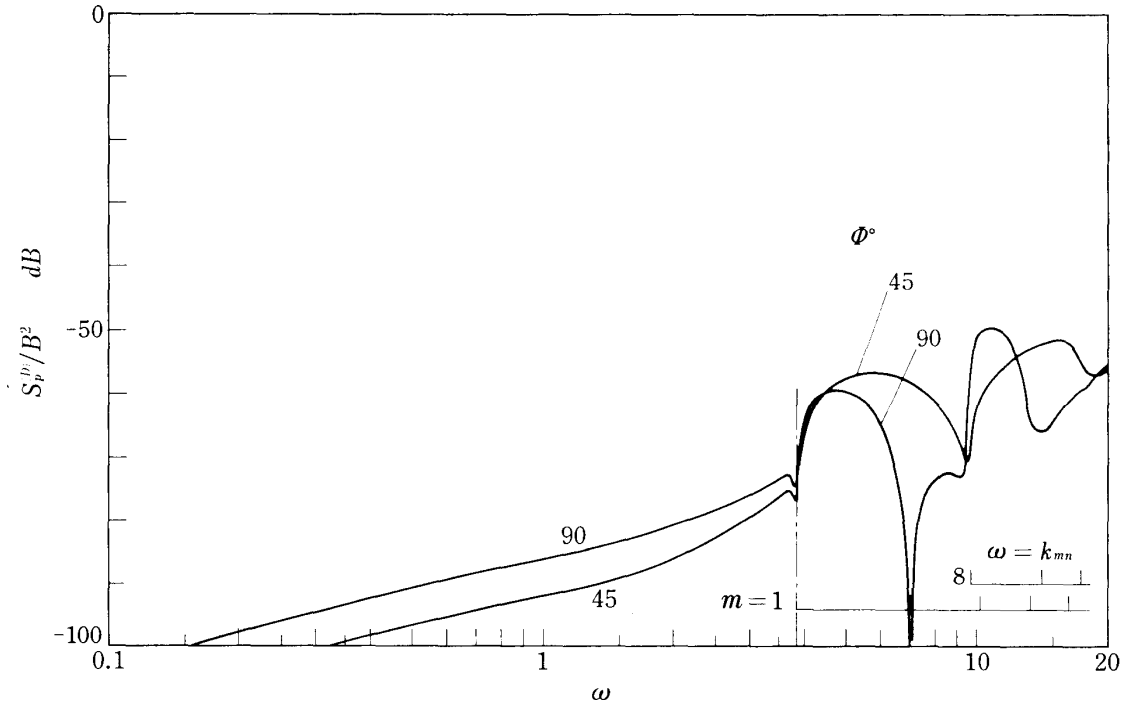

(c) Correlated turbulence, $B=8$.

FIG. 10. Frequency spectra of ducted-space fan noise without mean flow; $M=0$.

the open ends of duct, in order to examine their effect on the spectral density. The lowest cut-off frequency is denoted by a dot-dush line, below which the spectral density is dominated by decaying modes and above which it is attributed almost to propagating modes (see Fig. 10).

In the ducted-space case, even at $\Phi=90°$, the thrust component of fluctuating lift has a considerable effect upon the acoustic radiation through the J_0 term. The mechanism of noise generation hardly differs at the observation points in the far-field, so that spectra at $\Phi=90°$ and $\Phi=45°$ are almost same as shown in Fig. 10

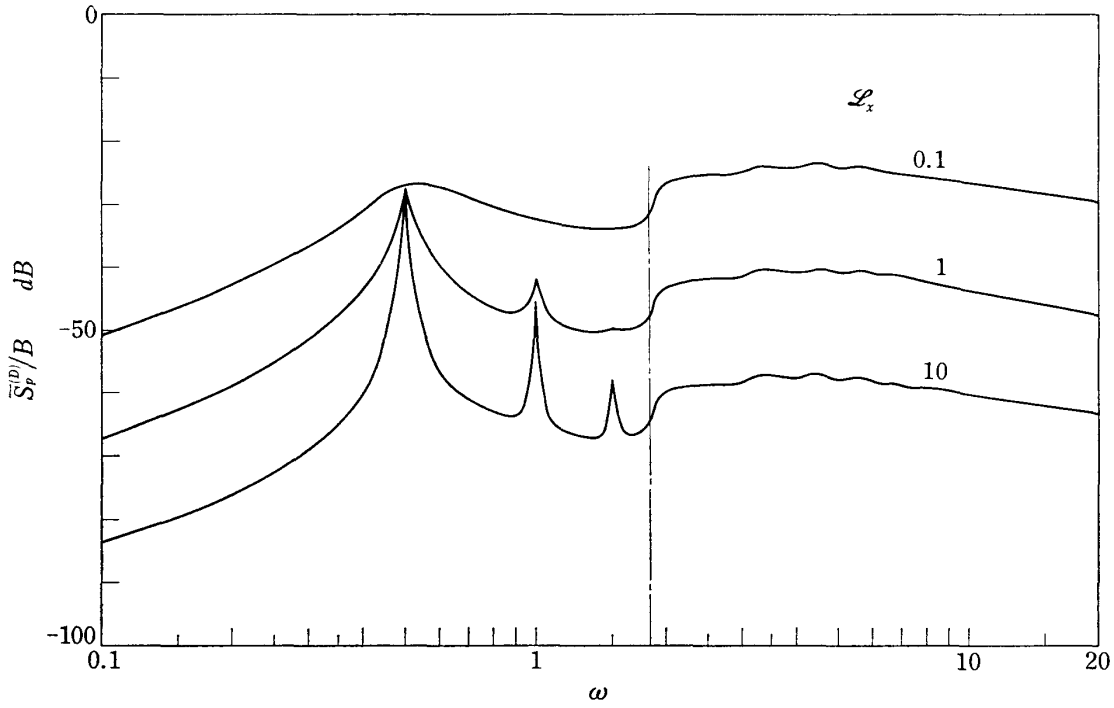

(a) Non-correlated turbulence.

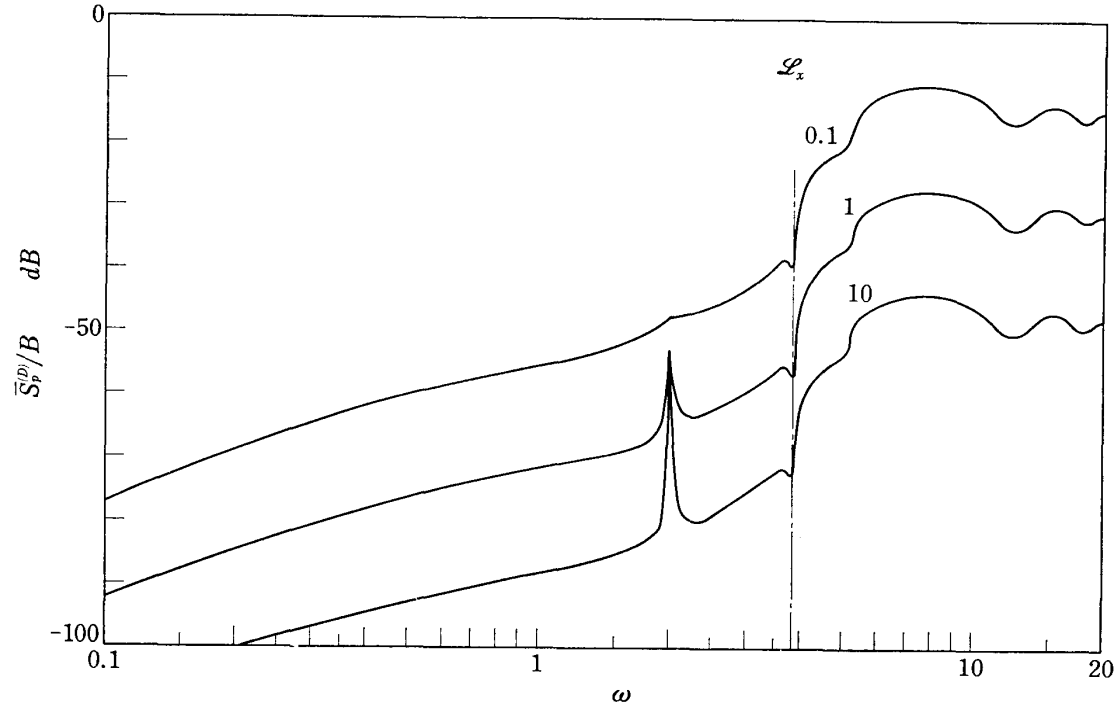

(b) Correlated turbulence, $B=4$.

FIG. 11. Effect of turbulence scale in ducted space; $M=0$, $\Phi=45°$.

(cf. Fig. 5). (The spectral density at $\Phi=0$, which is attributed only to the plane wave, is identical to that in the free-space case.) Above the cut-off frequency, the spectra are affected by complicated modal contributions. The peaks of spectra, corresponding to the frequency at which $k_{mn}^2-\omega^2\sin^2\Phi=0$ have a finite value, since

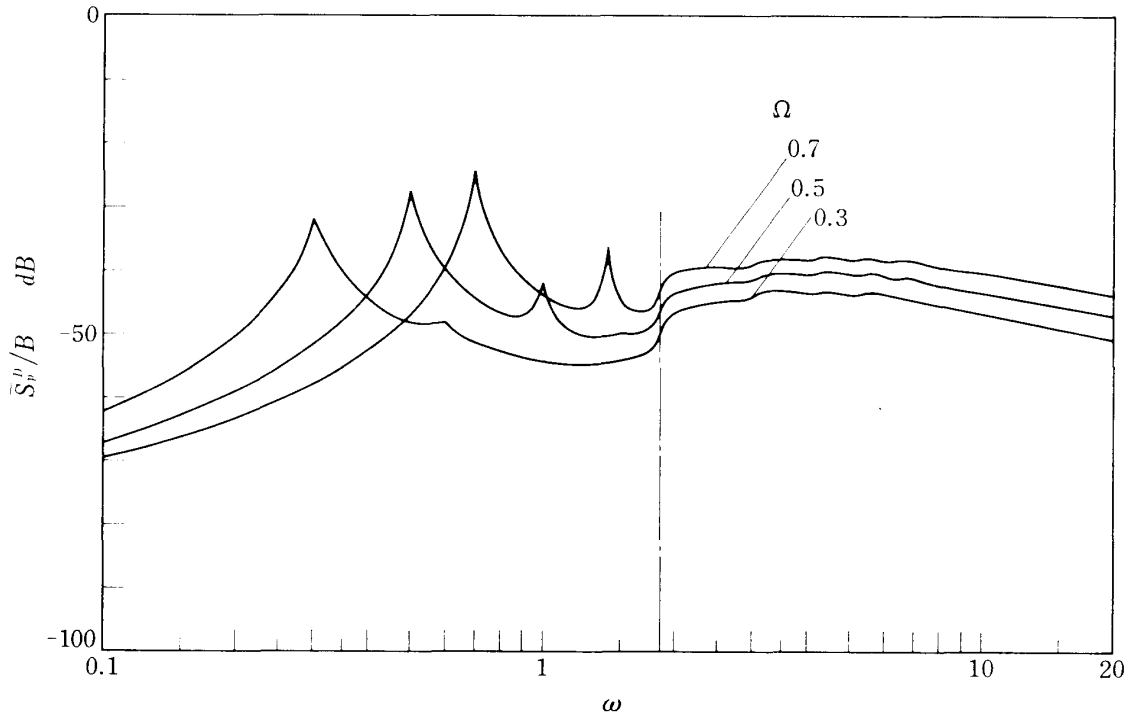

(a) Non-correlated turbulence.

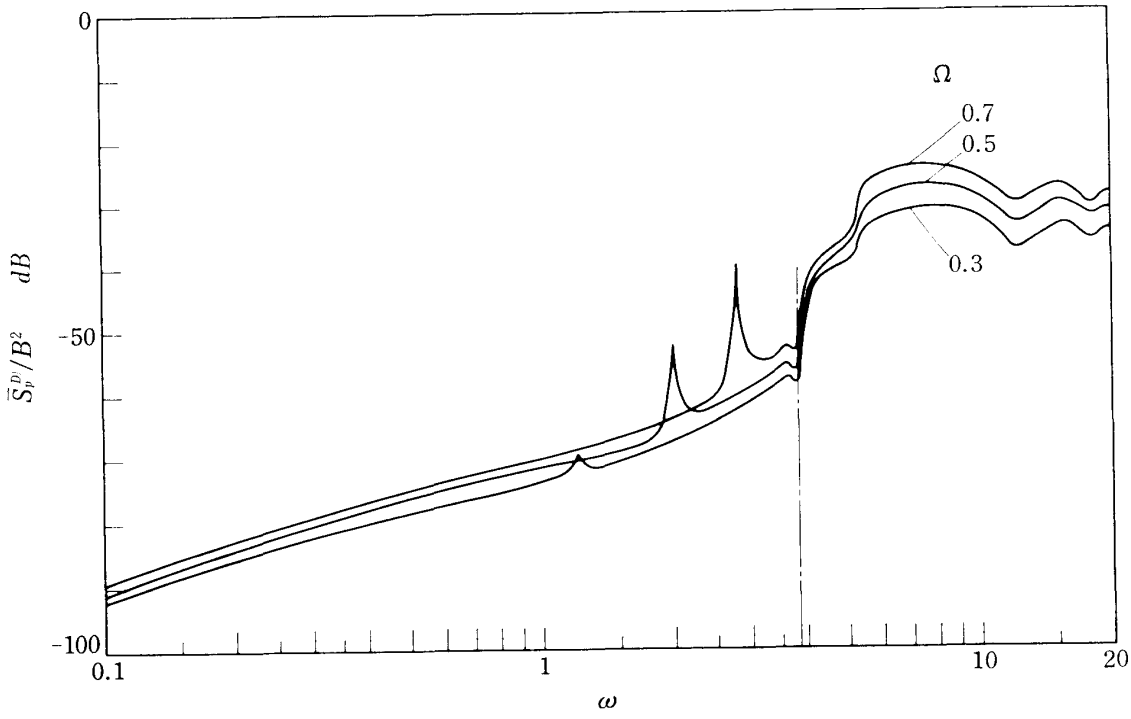

(b) Correlated turbulence, $B=4$.

FIG. 12. Effect of rotor speed in ducted space; $M=0$, $\Phi=45°$.

$$P_{mn}^{(D)}\left(\boldsymbol{x}, \omega=\frac{k_{mn}}{\sin\Phi}\right)=\frac{e^{\mp\kappa_{mn}l}}{2s_{mn}}J_m(k_{mn}R_e).$$

In Fig. 10, the mode cross-section wave numbers, k_{mn}, are shown. It is easily seen

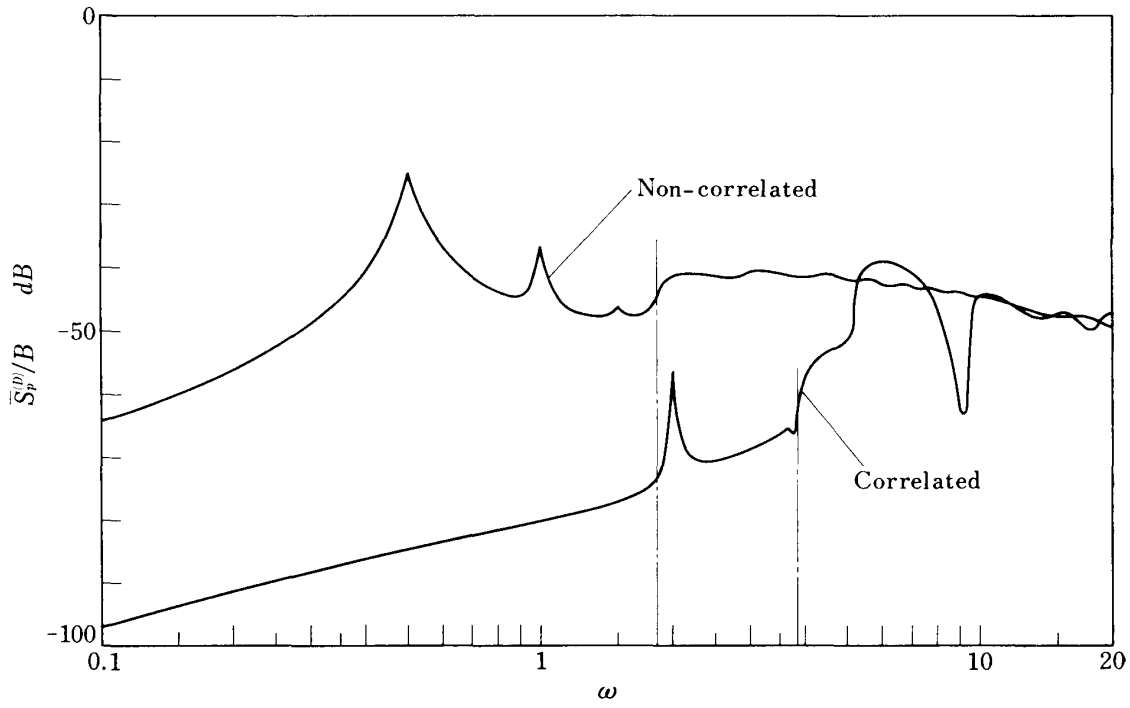

(a) $\Phi=45°$.

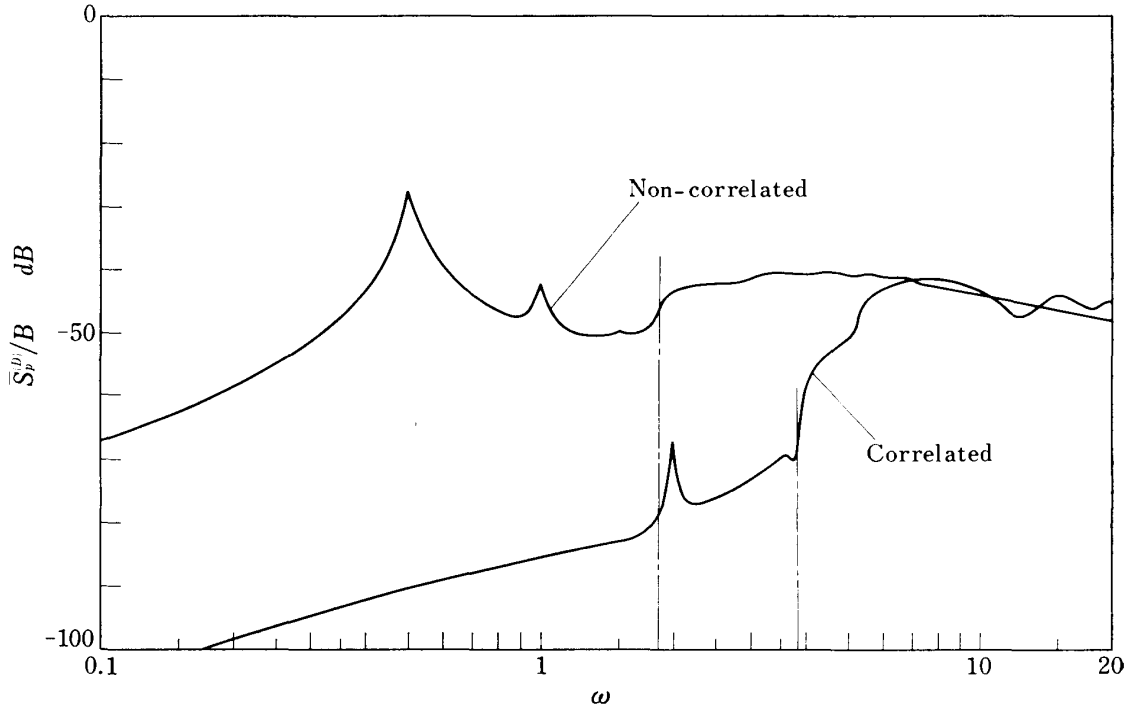

(b) $\Phi=90°$.

FIG. 13. Effect of turbulence correlation in ducted space; $M=0$, $B=4$.

that the spectrum mainly consists of "cut-on" modes of $(m, 0)$. For non-correlated turbulence (Fig. 10(a)), the lowest cut-off frequency of the J_0 term ($k_{01}=3.83$) is higher than those of the J_1 and J_2 terms ($k_{11}=1.84$, $k_{21}=3.05$) so that the contribution of the J_0 term is shaded behind those of higher order terms. On the contrary,

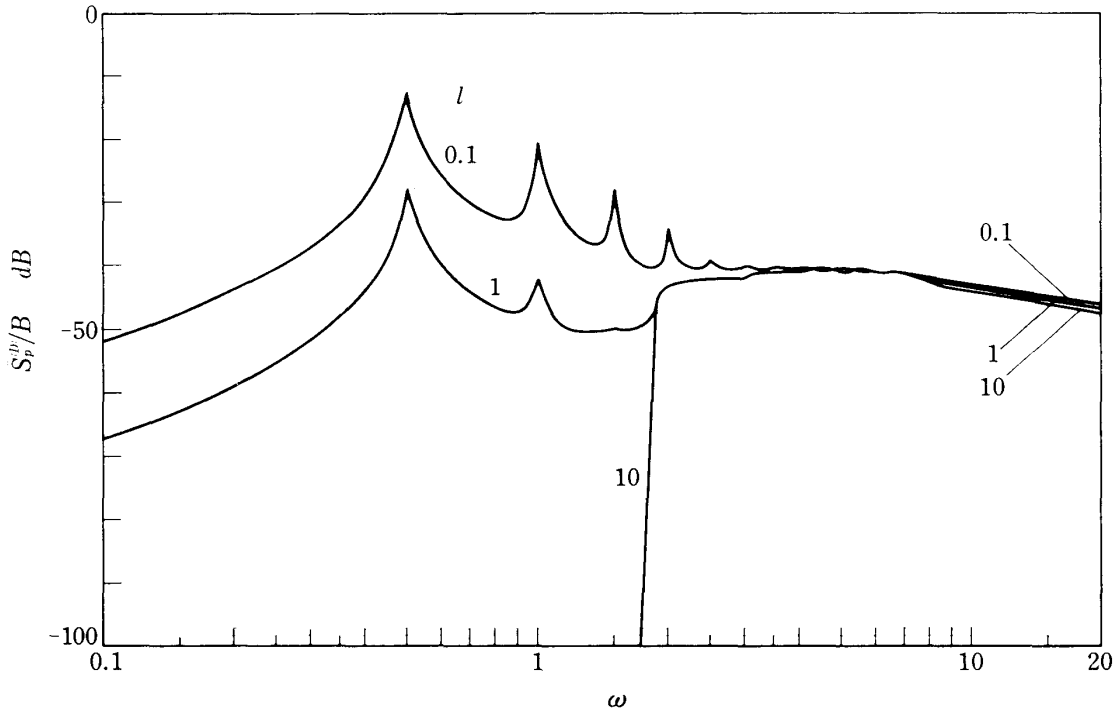

(a) Non-correlated turbulence.

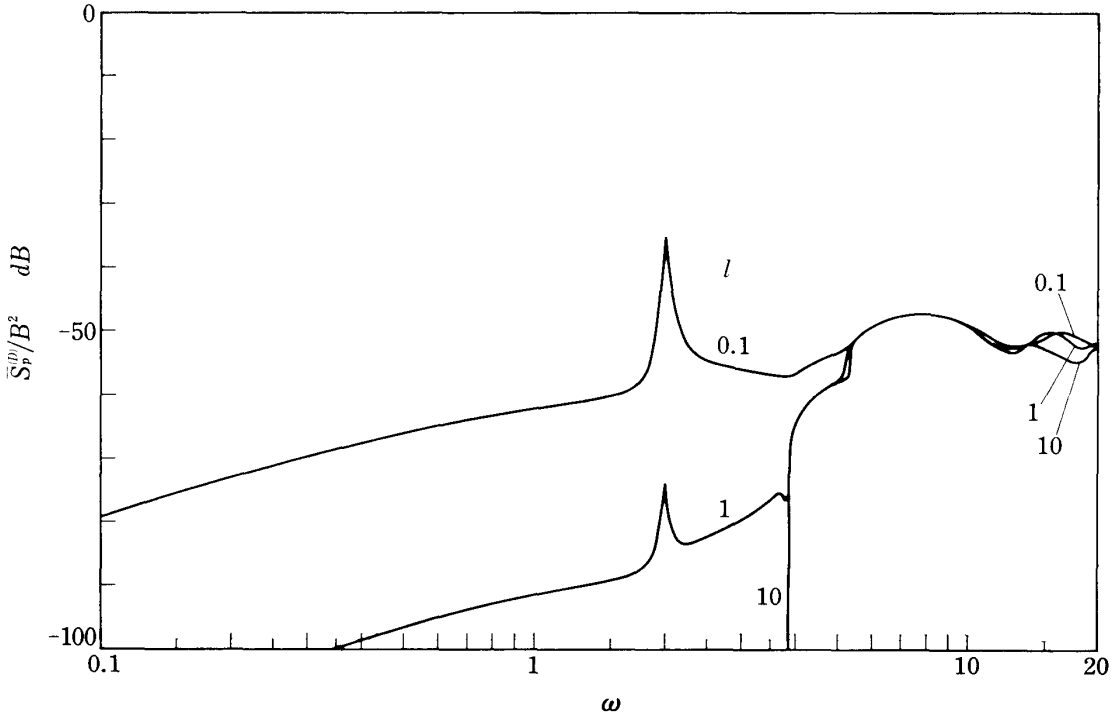

(b) Correlated turbulence, $B=4$.

FIG. 14. Effect of duct length in ducted space; $M=0$, $\Phi=45°$.

in the case of correlated turbulence (Figs. 10 (b) and (c)), the spectra are considerably characterized by the J_0 term.

The effect of axial turbulence scale on the spectrum above the cut-off frequency, as shown in Fig. 11, is only to shift it upward. It comes from the fact that the spectrum above the cut-off frequency is characterized almost by $P_{mn}^{(D)}$ rather than S_L which acts only as a constant factor. This features are also shown in Fig. 12 which represents the effect of rotor-speed.

Figure 13 shows the comparison of effects of non-correlated and correlated turbulences. As noted above, the former is affected by many modal contributions, especially by $(m, 0)$ modes, whereas the latter is dominated by a few modes, J_0 and J_4. It should be noted that inlet-turbulence with smaller circumferential scale could make the spectrum more flatten.

As shown in Fig. 14, the duct length larger than the duct radius has less influence upon the spectrum above the cut-off frequency, although the spectrum below it is much affected by decaying modes. In the case of non-correlated turbulence, for decaying modes to be decayed away sufficiently, the duct length is required to be $l \gtrsim 3 \sim 5$ whereas in the case of correlated turbulence $l \gtrsim 1$ is sufficient.

When the mean flow in the duct is taken into account, the features of decaying

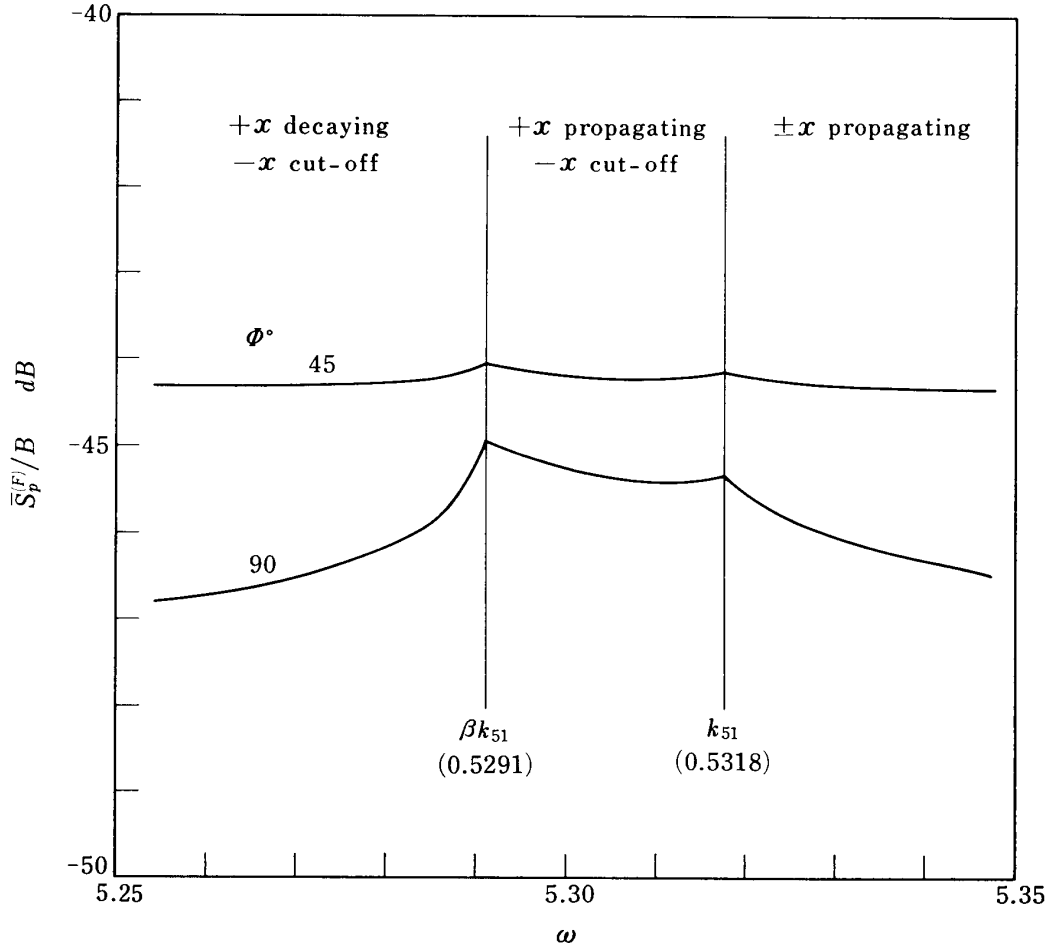

FIG. 15. Two cut-off modes with mean flow; $M=0.1$, $L=1$, $\mathscr{L}_x=1$, $\Omega=0.5$.

and propagating modes are much different from those without mean flow. As shown in Table 1, for $\omega > k_{mn}$, there are upward and downward propagating modes. For $k_{mn} \geqslant \omega \geqslant \beta k_{mn}$, there are upward propagating waves of two types with different propagating speeds and no waves exist in the downward direction. For $\omega < \beta k_{mn}$,

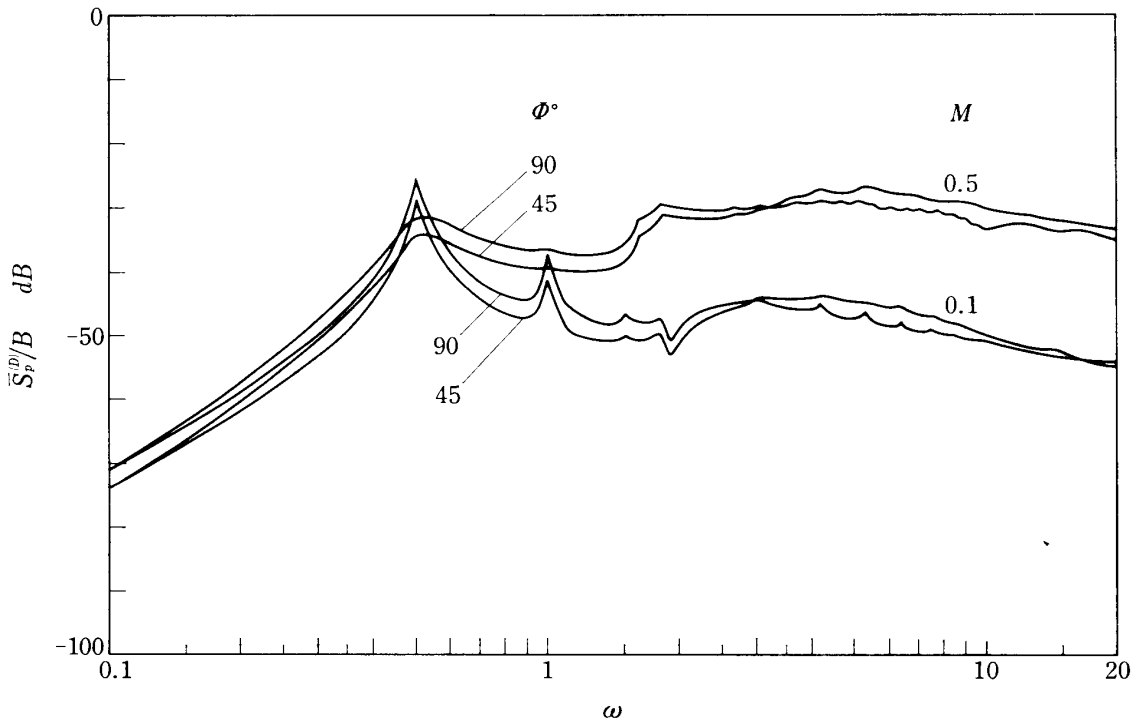

(a) Non-correlated turbulence.

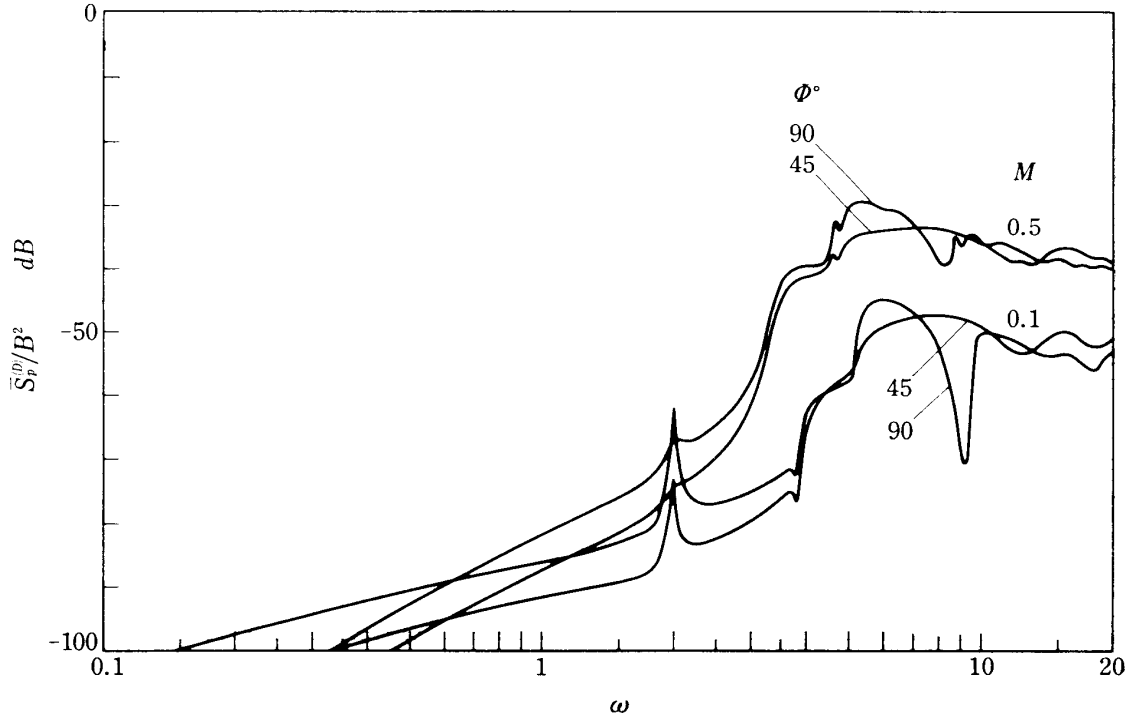

(b) Correlated turbulence, $B=4$.

FIG. 16. Frequency spectra of ducted-space fan noise with mean flow.

there is only an upward decaying mode. A typical example of this features is demonstrated in Fig. 15. All spectra for the case of no mean flow are modified by this features, although their main behavior remains almost same as that without mean flow (Fig. 16). The two cut-off frequencies, k_{mn} and βk_{mn} are more separated

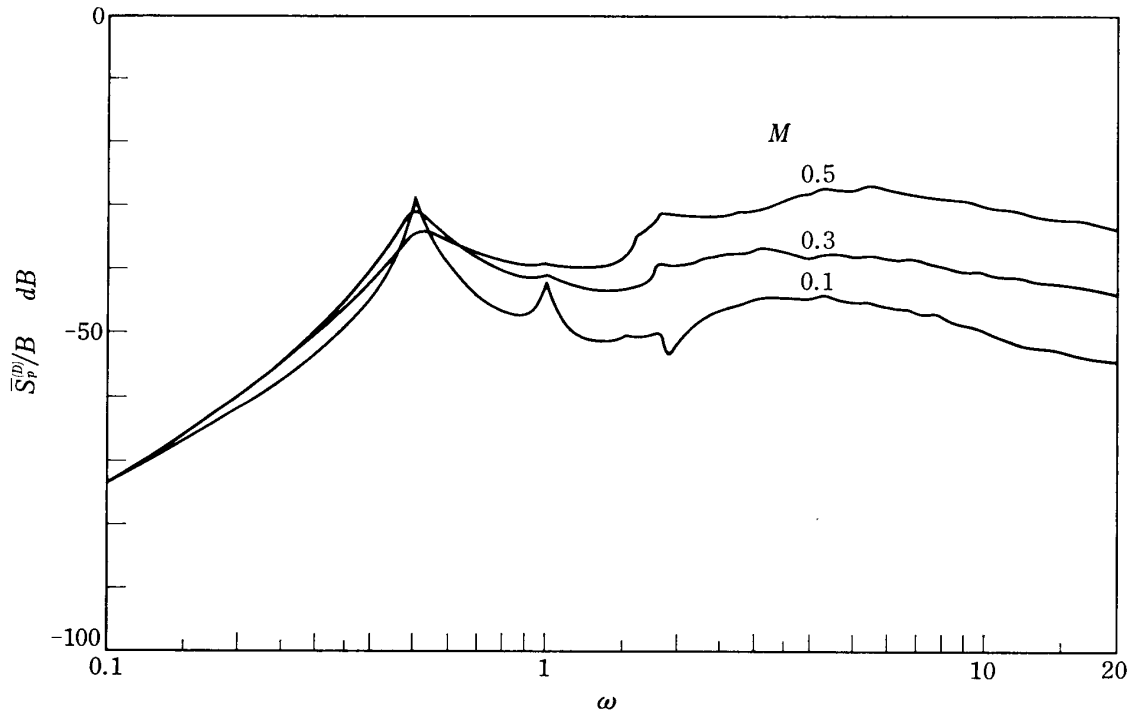

(a) Non-correlated turbulence.

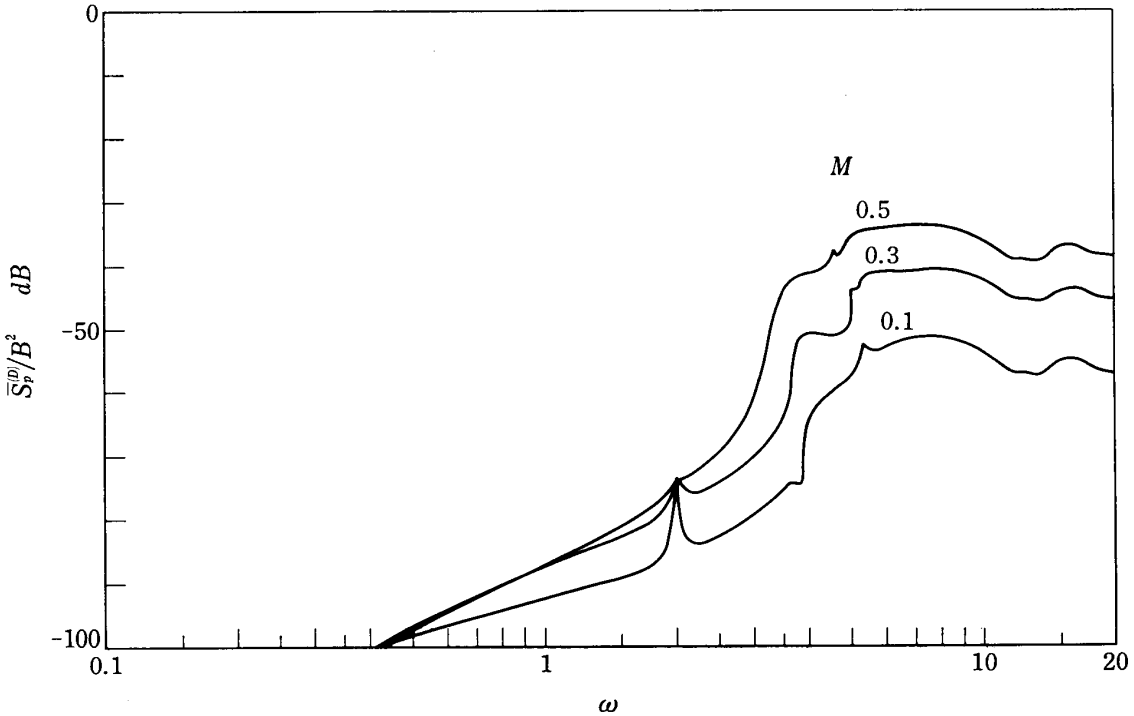

(b) Correlated turbulence, $B=4$.

FIG. 17. Effect of mean flow in ducted space; $\Phi=45°$.

with the increase of flow-velocity, so that the modification of spectra is remarkable at higher flow velocities (Fig. 17). The axial turbulence scale, the blade angle and the rotor-speed act only as shifting the spectrum upward without any change in its shape above the cut-off frequency (Fig. 18). The effect of the duct length is also

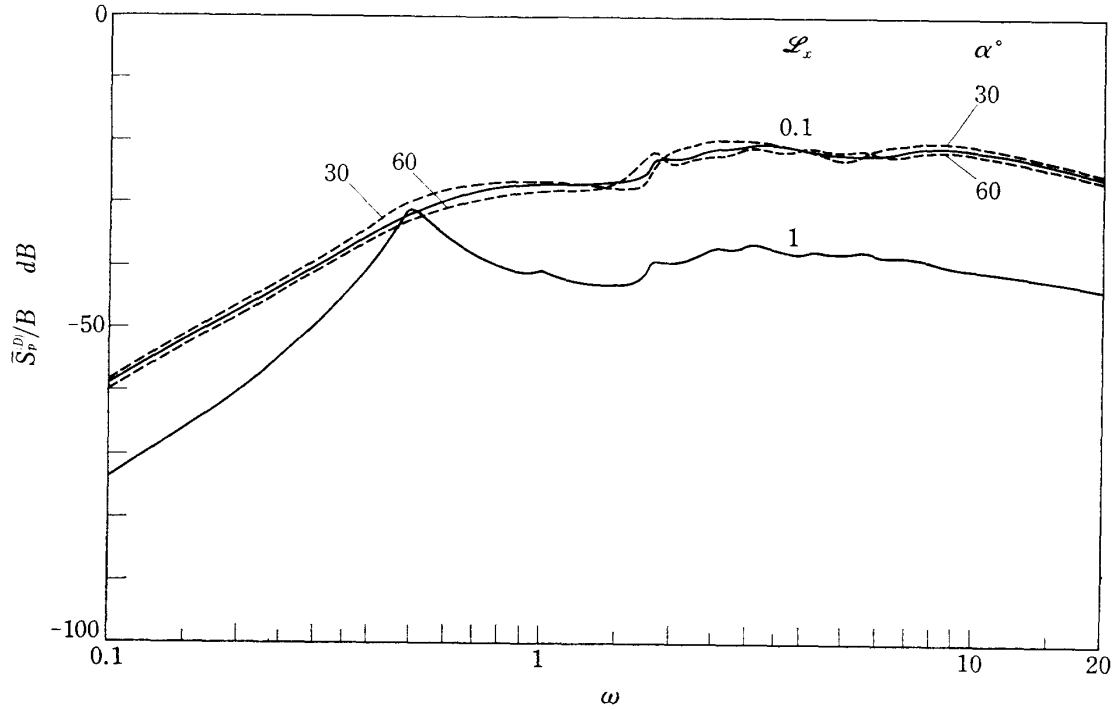

(a) Non-correlated turbulence.

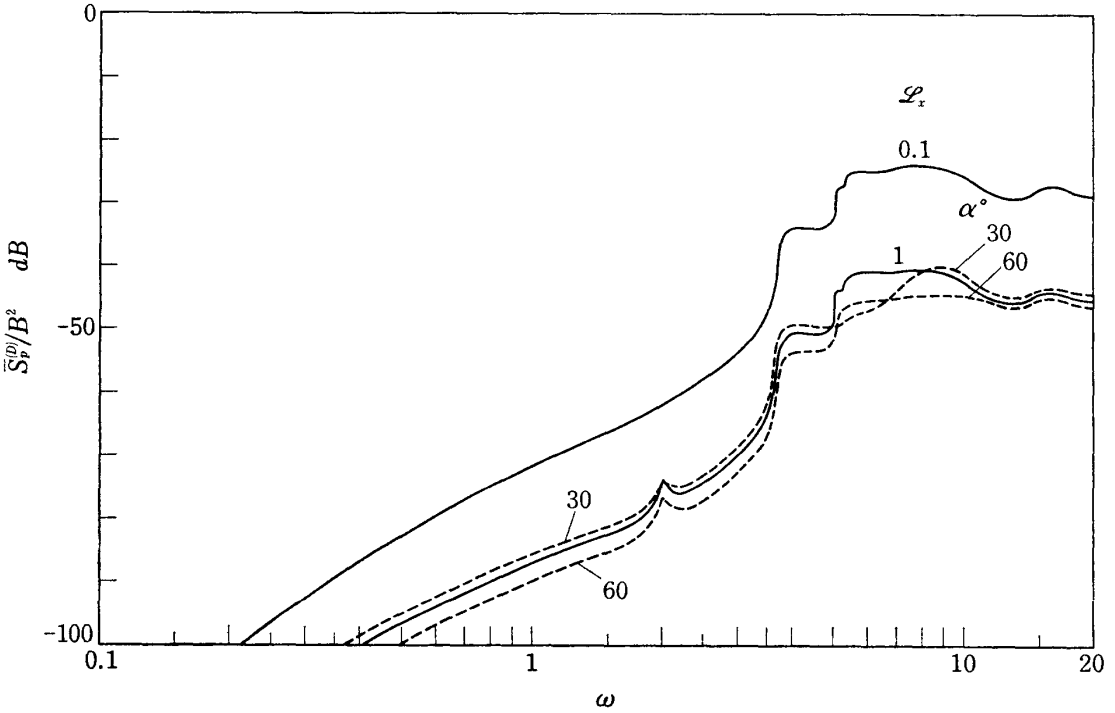

(b) Correlated turbulence, $B=4$.

FIG. 18. Effect of turbulence scale in ducted space; $M=0.3$, $\Phi=45°$.

similar as that without mean flow (Fig. 19).

The directivity is shown in Fig. 20. In this case, the directivity pattern is entirely symmetric, since the equivalent mass source distribution is assumed at the open ends of duct. Since the term of $P_{mn}^{(D)}$ in Eq. (61) can be rewritten as

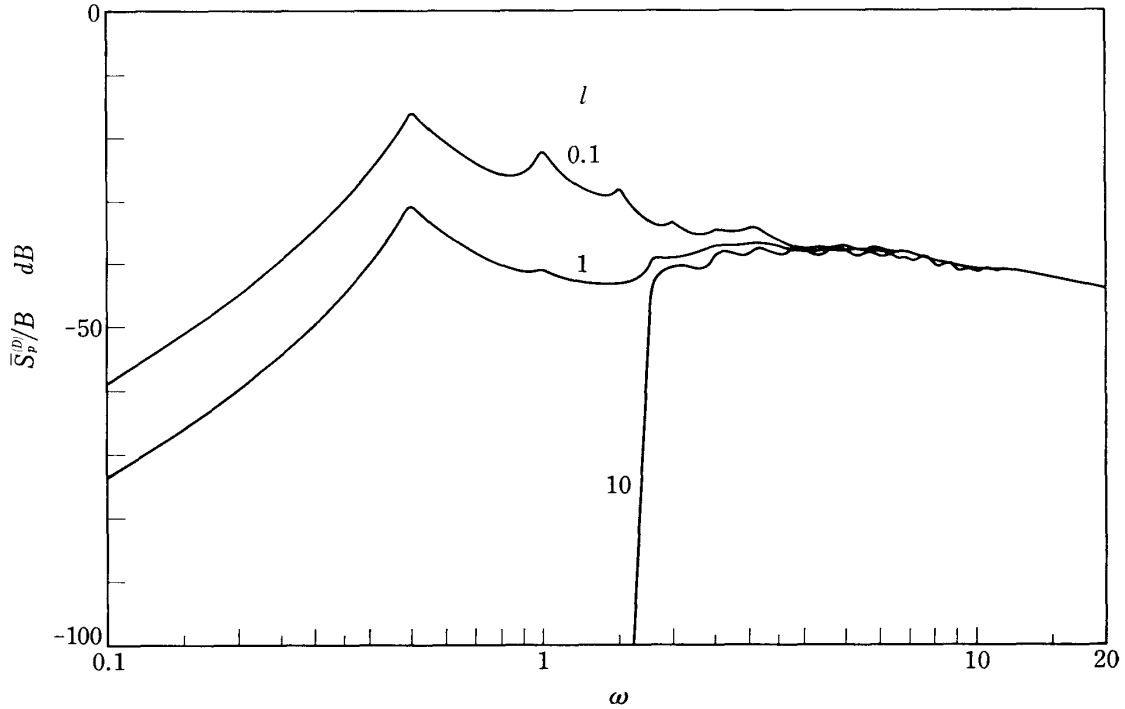

(a) Non-correlated turbulence.

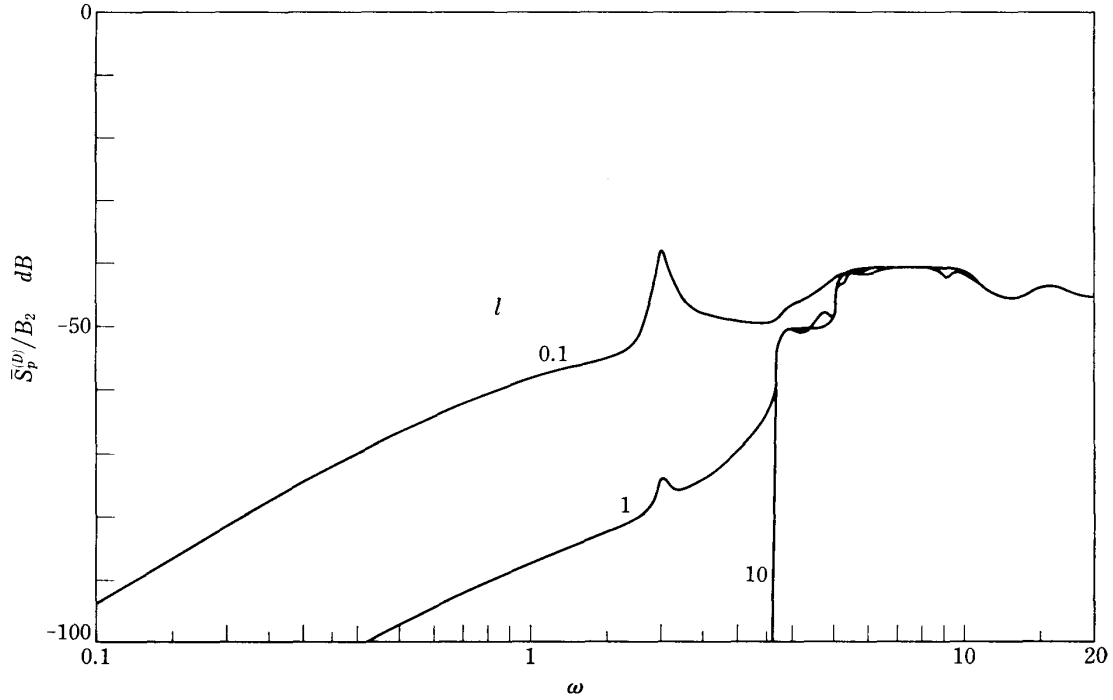

(b) Correlated turbulence, $B=4$.

FIG. 19. Effect of duct length in ducted space; $M=0.3$, $\Phi=45°$.

$$\omega \sin \Phi \cdot J_{m-1}(\omega \sin \Phi) - mJ_m(\omega \sin \Phi)$$
$$= \frac{1}{2}\omega \sin \Phi \{J_{m-1}(\omega \sin \Phi) - J_{m+1}(\omega \sin \Phi)\}$$

the directivity behaves like $(\sin \Phi)^{0\sim4}$, except for the axial direction $\Phi = 0$ where only plane wave can exist. The axial turbulence scale, the duct length and the mean flow velocity have less effect on the directivity pattern, especially above the cut-off frequencies, although their absolute values are affected by them. The acoustic power for correlated turbulence is always smaller than that for non-correlated turbulence due to less modal contribution, especially close to the axial direction. It is interesting to note that correlated turbulence could emit more sound toward the rotor plane in a ducted space than in a free space, although correlated turbulence radiates absolutely more sound in a free space. It comes mainly from the difference of contribution of the J_0 term.

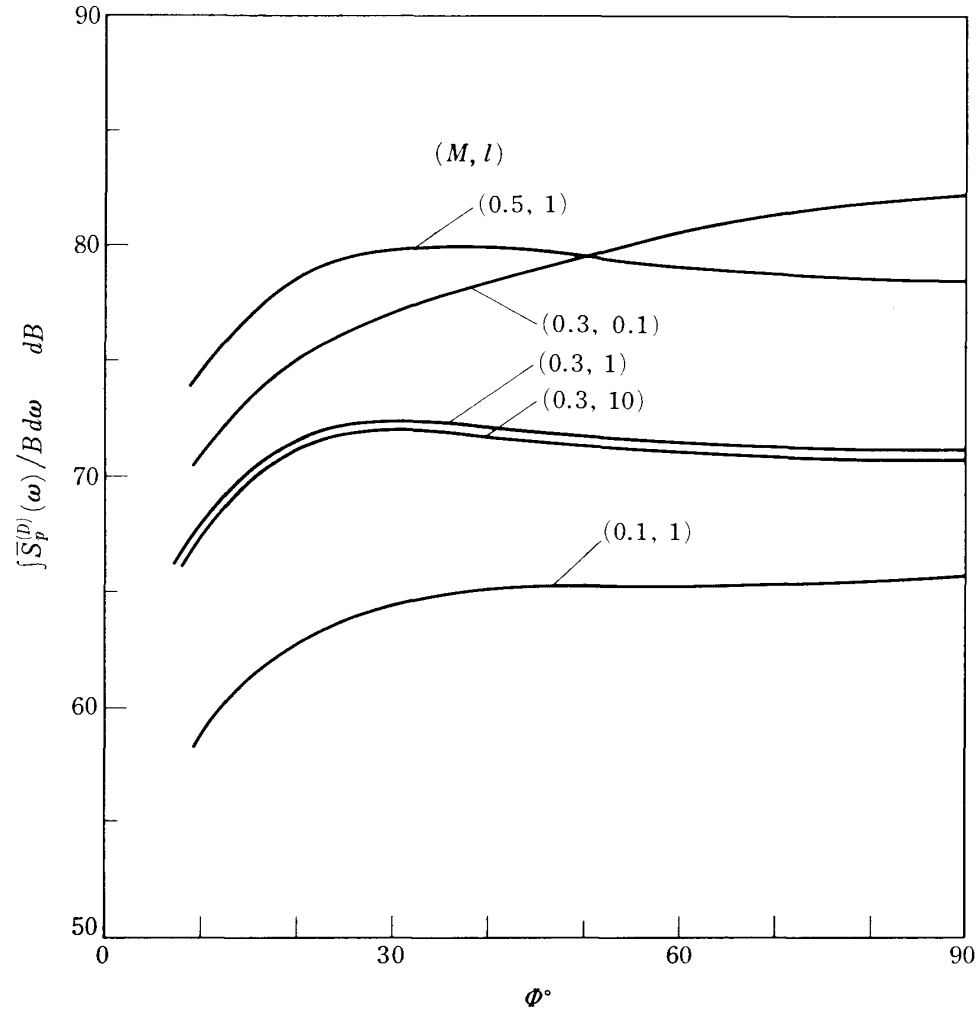

(a) Non-correlated turbulence.

FIG. 20. Directivity of sound pressure in ducted space.

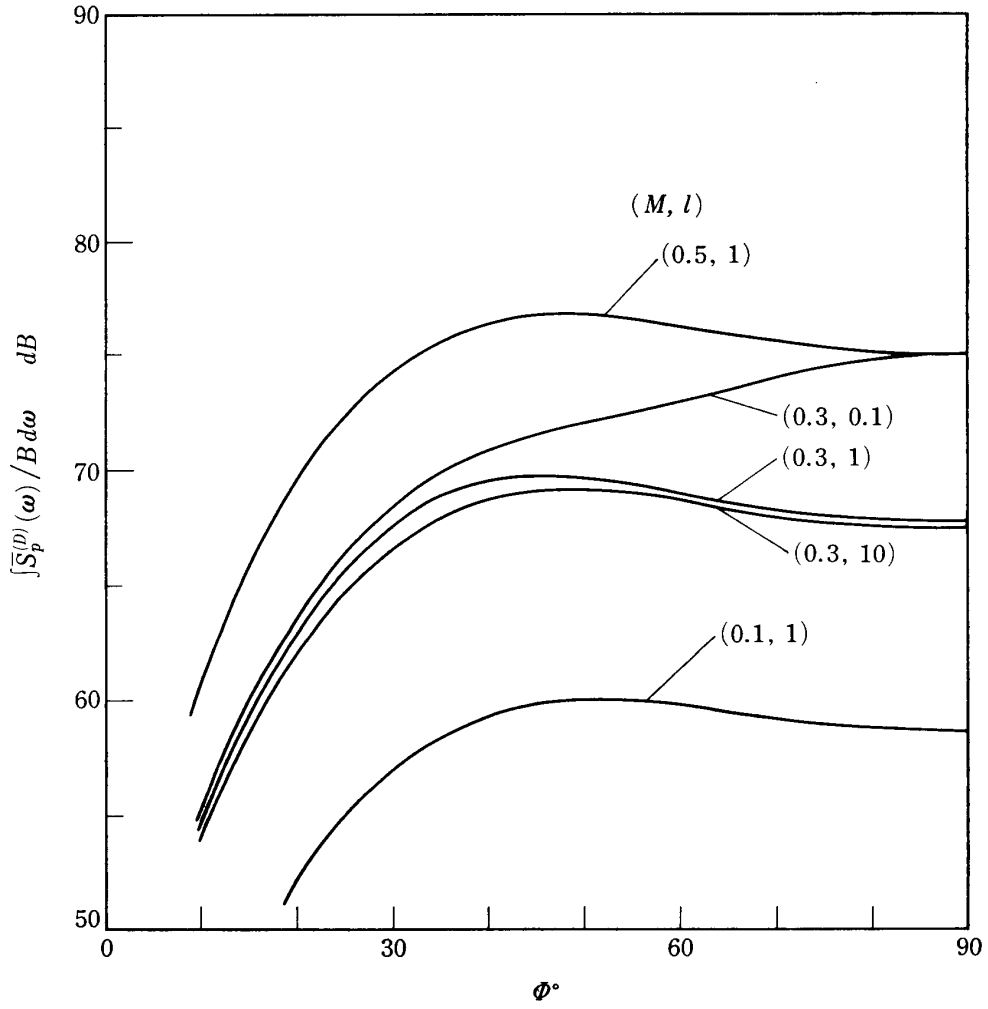

(b) Correlated turbulence, $B=4$.

FIG. 20. Directivity of sound pressure inducted space.

7. CONCLUDING REMARKS

By assuming incompressible two-dimensional aerodynamic response of point-concentrated life to homogeneous inlet-turbulence and neglecting the effect of duct termination, the far-field acoustic radiation caused by inlet-turbulence/rotor interaction is theoretically investigated for cases of a rotor operating in free-space and in ducted-space. Although, due to these considerable simplification, the obtained results might have restricted validity, they show a number of interesting and significant aspects of the sound fields.

The spectral density of the far-field sound power in free-space can be largely affected by the nature of turbulence, especially, by the circumferential correlation scale. With circumferentially non-correlated inlet-turbulence, the associated spectrum has harmonics of the rotational frequency of the rotor, whereas well-correlated turbulence makes harmonics of the bladepassing frequency. Decreasing axial turbulence scale broadens the band width of these harmonic peaks due to less sharped aerodynamic response spectrum. The additive effect of thrust-term radiation toward the axial

direction and torque-term radiation close to the rotor-plane results in a rather flat directivity pattern.

In the case of rotor operating in a ducted space, the power spectral densities of associated sound are much different from those for the free-sapce case due to complicated contributions of duct modes. Above the cut-off frequency, the spectrum is characterized mainly by the $(m, 0)$ modes and hardly affected by axial turbulence scale, rotor-speed and decaying modes (duct length), which have an effect only to shift the spctrum. Increasing mean flow velocity in the duct results in spectrum having two peaks for each $(m, 0)$ mode corresponding to two types of cut-off mode. The far-field radiation for the ducted-space case is more emitted close to the rotor-plane, being not always less than that for the free-space case.

In the present analysis, the key step for the ducted-space case was to determine the acoustic modes of the duct of infinite length, which means that any solution must contain only modes travelling away from the sources. However, in general, there exist modes reflected at the termination of duct, which imply that acoustic field inside a duct must be determined not only by the inside solution, but by coupling it with the outside solution. The duct termination has a considerable effect upon the acoustic radiation of sound generated inside a duct, especially at frequencies below and close to the cut-off.

In addition to this, the reflection at the duct termination provides its interaction with the aerodynamic behavior of rotating blades, which requires consideration on the compressibility effect. Since the excitation and transmission of sound in a duct space should be controlled by the nature of the space-time pattern of the source distribution, its three-dimensionality must also be studied.

Further numerical works concerning these subjects are urgently required to obtain the appreciable prediction and control of fan-noise problems associated with duct systems.

Acknowledgements

The author wishes to express his gratitude to Prof. G.W. Johnston who provided the opportunity of the present work and to Mr. D. Noble for his helpful advice and discussions through the work.

Department of Propulsion.
Institute of Space and Aeronautical Science
University of Tokyo
October 29, 1980

References

[1] Mani, R. Noise due to interaction of inlet turbulence with isolated stators and rotors, J. Sound and Vibration **17**, 1971, pp. 251–260.

[2] Chandrashekhara, N. Tone radiation from axial flow fans running in turbulent flow, J. Sound and Vibration **18**, 1971, pp. 533–543.

[3] Hanson, D. B. The spectrum of turbomachine rotor noise caused by inlet guide vane wakes and atmospheric turbulence, Hamilton Standard Division, United Aircraft Corporation, HSER 6191, 1973.
[4] Amiet, R. K. Acoustic radiation from an airfoil in a turbulent stream, J. Sound and Vibration **41**, 1975, pp. 407–420.
[5] Doak, P. E. Excitation, transmission and radiation of sound distribution in hard-walled ducts of finite length, (I) The effects of duct cross-section geometry and source distribution space-time pattern, J. Sound and Vibration **31**, 1973, pp. 1–72; (II) The effects of duct length, J. Sound and Vibration **31**, 1973, pp. 137–174.
[6] Ogimoto, K. Sound radiation from a finite length unflanged circular duct with uniform axial flow, Institute for Aerospace Studies, University of Toronto, UTIAS Report No. 231, 1980.
[7] Teunissen, H. W. Characteristics of the mean wind and turbulence in the planetary boundary layer, Institute for Aerospace Studies, University of Toronto, UTIAS Review No. 32, 1970.
[8] Kemp, N. H. and Sears, W. R. The unsteady forces due to viscous wakes in turbomachines, J. Aerospace Science **22**, 1955, pp. 478–483.
[9] Kemp, N. H. On the lift and circulation of airfoils in some unsteady flow problems, J. Aerospace Science **19**, 1952, p. 713.

Appendix A. Green's function for an infinite circular duct with flow.

The Green's function is defined as a solution of Eqs. (8) and (9),

$$\nabla^2 g(\boldsymbol{r}, t; \boldsymbol{r}_0, t_0) - \frac{1}{a^2}\left(\frac{\partial}{\partial t} - U\frac{\partial}{\partial x}\right)^2 g(\boldsymbol{r}, t; \boldsymbol{r}_0, t_0) = -\delta(\boldsymbol{r}-\boldsymbol{r}_0)\delta(t-t_0) \quad \text{(A1)}$$

subject to the boundary condition at $r=R$

$$\frac{\beta_w}{a}\left(\frac{\partial}{\partial t} - U\frac{\partial}{\partial x}\right) g(\boldsymbol{r}, t; \boldsymbol{r}_0, t_0) = -\frac{\partial}{\partial r} g(\boldsymbol{r}, t; \boldsymbol{r}_0, t_0). \quad \text{(A2)}$$

In the Fourier transform, these are

$$\nabla^2 G(\boldsymbol{r}; \boldsymbol{r}_0, \omega) - \left(ik - M\frac{\partial}{\partial x}\right)^2 G(\boldsymbol{r}; \boldsymbol{r}_0, \omega) = -\delta(\bar{r}-\bar{r}_0) \quad \text{(A3)}$$

$$\beta_w\left(ik - M\frac{\partial}{\partial x}\right) G(\boldsymbol{r}; \boldsymbol{r}_0, \omega) = -\frac{\partial}{\partial r} G(\boldsymbol{r}; \boldsymbol{r}_0, \omega) \qquad r=R. \quad \text{(A4)}$$

Assuming a solution in the form

$$G(\boldsymbol{r}; \boldsymbol{r}_0, \omega) = X(x, \omega)\Phi(r)\Theta(\theta), \quad \text{(A5)}$$

one obtains the following equations.

$$(1-M^2)\frac{\partial^2 X}{\partial x^2} + 2ikM\frac{\partial X}{\partial x} - (k^2 - K^2)x = 0$$

$$\frac{d^2\Phi}{dr^2} + \frac{1}{r}\frac{d\Phi}{dr} + \left(K^2 - \frac{m^2}{r^2}\right)\Phi = 0$$

$$\frac{d^2\Theta}{d\theta^2} + m^2\Theta = 0$$

The solutions for Φ and Θ are Bessel and sinusoidal functions, respectively;

$$\Phi(r)=J_m(kr) \qquad \Theta(\theta)=e^{im\theta}.$$

The solution for X is given by

$$\begin{aligned} X(x)&=e^{-i\kappa x} \\ \kappa&=\frac{1}{\beta^2}\{kM\pm\sqrt{k^2-\beta^2K^2}\} \qquad \beta=\sqrt{1-M^2} \end{aligned} \tag{A6}$$

With X in this form, the boundary condition is

$$i\beta_w(k+\kappa M)J_m(KR)=-\left.\frac{dJ_m(Kr)}{dr}\right|_{r=R} \tag{A7}$$

which gives the consecutive values of K for each m;

$$K=k_{mn} \qquad (m=0,\ \pm1,\ \pm2,\cdots,\infty,\ n=0,\ 1,\ 2,\cdots\infty)$$

When only waves travelling away from the sources are considered, κ/k must be positive for $x-x_0>0$ and negative for $x-x_0<0$. This leads to the κ_{mn} value shown in Table 1.

The Green's function can then be expressed as

$$G(\boldsymbol{r};\boldsymbol{r}_0,\omega)=\sum_{m=-\infty}^{\infty}\sum_{n=0}^{\infty}G_{mn0}J_m(k_{mn}r)e^{im\theta}e^{-i\kappa_{mn}x} \tag{A8}$$

Substituting Eq. (A8) into (A3), multiplying by the complex conjugate of $rJ(k_{mn}r)e^{-im\theta}$ and integrating with respect to $r=0\sim R$, $\theta=0\sim2\pi$ and $x=(x_0-\varepsilon)\sim(x_0+\varepsilon)$ with $\varepsilon\to0$, one obtains

$$G_{mn0}=\frac{1}{i2\pi R^2}\frac{1}{\Lambda_{mn}s_{mn}}J_m(k_{mn}r_0)e^{-im\theta_0}e^{i\kappa_{mn}x_0}$$

where

$$\begin{aligned} \Lambda_{mn}&=\left(1-\frac{m^2}{k_{mn}^2R^2}\right)J_m^2(k_{mn}R)+\{J_m'(k_{mn}R)\}^2 \\ s_{mn}&=\frac{\beta^2}{2}\{(\kappa_{mn})_{x-x_0>0}-(\kappa_{mn})_{x-x_0<0}\} \end{aligned}$$

The explicit expression of s_{mn} is shown in Table 1.

Appendix B. Approximation of Sears function

The power spectral density of lift response of Sears function is given by Eq. (48),

$$S_e(\bar{\omega})=\left(\frac{\pi\bar{\omega}}{2}\right)^{-2}[\{J_0(\bar{\omega})-Y_1(\bar{\omega})\}^2+\{Y_0(\bar{\omega})+J_1(\bar{\omega})\}^2]^{-1} \tag{48}$$

For $\bar{\omega}<1$, $J_0(\bar{\omega})$, $J_1(\bar{\omega})$, $Y_0(\bar{\omega})$ and $J_1(\bar{\omega})$ are expanded with respect to $\bar{\omega}$ as

$$J_0(\bar{\omega})=1-\frac{1}{8}\bar{\omega}^2+\cdots$$

$$J_1(\bar{\omega})=\frac{1}{2}\bar{\omega}-\frac{1}{48}\bar{\omega}^3+\cdots$$

$$Y_0(\bar{\omega})=\frac{2}{\pi}J_0(\bar{\omega})(\Gamma+\ln\bar{\omega}) \qquad \Gamma=0.276186$$

$$Y_1(\bar{\omega})=\frac{2}{\pi}J_1(\bar{\omega})(\Gamma+\ln\bar{\omega})$$

These approximation leads to

$$S_e(\bar{\omega})=\{R^2+I^2\}^{-1} \tag{B1}$$

$$R=1+\frac{\pi}{2}\bar{\omega}-\frac{1}{2}\left(\Gamma-\frac{1}{2}+\ln\bar{\omega}\right)\bar{\omega}^2$$

$$I=(\Gamma+\ln\bar{\omega})\bar{\omega}+\left(\frac{\pi}{4}-\frac{1}{8}\bar{\omega}\ln\bar{\omega}\right)\bar{\omega}^2$$

For $\bar{\omega}>1$, $J_0(\bar{\omega})$, $J_1(\bar{\omega})$, $Y_0(\bar{\omega})$ and $Y_1(\bar{\omega})$ are approximated as

$$J_0(\bar{\omega})=\sqrt{\frac{2}{\pi\bar{\omega}}}\cos\left(\bar{\omega}-\frac{\pi}{4}\right) \qquad J_1(\bar{\omega})=\sqrt{\frac{2}{\pi\bar{\omega}}}\cos\left(\bar{\omega}-\frac{3\pi}{4}\right)$$

$$Y_0(\bar{\omega})=\sqrt{\frac{2}{\pi\bar{\omega}}}\sin\left(\bar{\omega}-\frac{\pi}{4}\right) \qquad Y_1(\bar{\omega})=\sqrt{\frac{2}{\pi\bar{\omega}}}\sin\left(\bar{\omega}-\frac{3\pi}{4}\right)$$

which yield

$$S_e(\bar{\omega})=\frac{1}{2\pi\bar{\omega}} \tag{B2}$$

The power spectral density of approximated Sears functions, (B1) and (B2) is shown in Fig. 3, and compared with exact Sears function, Eq. (48), and with Liepmann's approximation (H.W. Liepmann, J. Aeronautical Sciences, vol. 19, 793–800, 1952). From the figure, it is seen that $S_e(\bar{\omega})$ is well approximated by Eqs. (B1) and (B2) for $\bar{\omega}\leqslant 0.9$ anld $\bar{\omega}\geqslant 0.9$, respectively.